AD-A127 517 ROCKETBORNE MEASUREMENTS OF OPTICAL EMISSIONS FROM THE AURORAL E-LAYER(U) AIR FORCE GEOPHYSICS LAB HANSCOM AFB MA R A VAN TASSEL 16 NOV 82 AFGL-TR-82-0354 1/1

UNCLASSIFIED F/G 14/2 NL

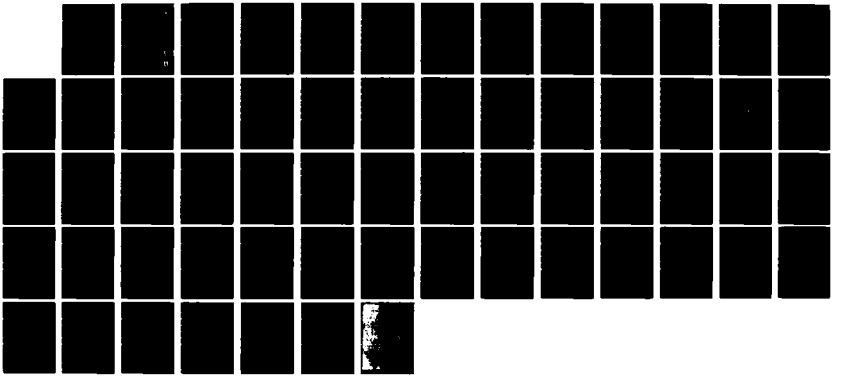

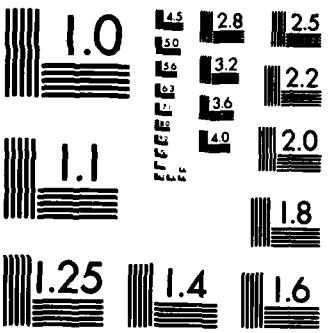

AFGL-TR-82-0354
ENVIRONMENTAL RESEARCH PAPERS, NO. 807

Rocketborne Measurements of Optical Emissions From the Auroral E-Layer

R.A. VAN TASSEL

16 NOVEMBER 1982

AERONOMY DIVISION PROJECT 6690
AIR FORCE GEOPHYSICS LABORATORY
HANSCOM AFB, MASSACHUSETTS 01731

AIR FORCE SYSTEMS COMMAND, USAF

This report has been reviewed by the ESD Public Affairs Office (PA) and is releasable to the National Technical Information Service (NTIS).

This technical report has been reviewed and is approved for publication.

Alva T Stair, Jr.

DR. ALVA T. STAIR, Jr
Chief Scientist

Qualified requestors may obtain additional copies from the Defense Technical Information Center. All others should apply to the National Technical Information Service.

REPORT DOCUMENTATION PAGE

AD-A192 517

DD 1473

20. (Contd)

profiles and assessments of ground return. Plots of column emission vs time, and vs altitude on ascent and descent are included for comparison with the results of model calculations.

Preface

We wish to thank the many personnel who contributed to the success of this rocket experiment. In particular we appreciate the willing support of the personnel of the Poker Flats Research Range, Mr. John M. Otis of the AFGL Sounding Rocket Branch who integrated the photometers into the rocket payload and thoroughly tested the system, and to Mr. Robert J. Raistrick of the AFGL Computation Branch who provided timely analytic support and data management.

Contents

Illustrations

Tables

Rocketborne Measurements of Optical Emissions From the Auroral E-Layer

I. INTRODUCTION

The overall objective of the AFGL Auroral-E Program is to develop a system to specify the electron density in the auroral E-layer by remote sensing of optical emissions. The first step in meeting this objective was a careful input-output experiment conducted in Alaska during March 1971. This experiment included satellite measurements of the source particle streams; rocket measurements of the optical emissions, electron and proton fluxes and electron, neutral and ion densities, neutral winds and electromagnetic fields; airborne measurements to provide data to assess the auroral and ionospheric conditions prior to and during launch; and incoherent scatter radar measurements to provide neutral wind, electric field and electron density data. These data will be used to establish a quantitative relationship among the precipitating particles, the resulting electron density profiles and the optical emissions from several species in the continuous or diffuse aurora. This report gives the results of the rocketborne filter photometer experiment.

The emissions observed were the N_2^+ First Negative (1N) system at 3914 Å, the N_2 Second Positive (2P) system at 3371 Å, the N_2 Vegard-Kaplan system at 2750 Å, $O(^1s\text{-}^3P)$ at 2761 Å, H_β at 4861 Å, and the underlying continuum at 5080 Å. Measurements of H_β were used to determine the degree of proton precipitation

---

Received for publication 12 November 1971

producing the aurora while the continuum gives an upper limit to the product of [NO] and [O] since it is attributed to the air afterglow reaction.

The photometers were used in an up-down configuration to produce detailed vertical profiles and assessments of ground return. Six photometers viewed in the forward direction and hence upward, while six others viewed aft or downward. They were mounted with their optic axes parallel to the spin axis of the rocket. The photometer designations and observed spectral features and their wavelengths are indicated in Table 1. The designation PF refers to the forward-mounted, upward-viewing photometers, while PA refers to the aft-mounted downward-viewing instruments. The up-down configuration allows calculation of the total intensity of the features studied along a line parallel to the rocket axis as well as their altitude profiles.[1] It also allows an assessment of the ground return.

Table 1. Filter Photometer Designations, Viewing Direction and Observed Spectral Feature

Photometer Designation	Viewing Direction	Wavelength Å	Spectral Feature
PF1	Forward	2761	N_2 Vegard-Kaplan (0, 6)
PF2	Forward	3371	N_2 Second Positive (0, 0)
PF3	Forward	3914	N_2^+ First Negative (0, 0)
PF4	Forward	4861	Hydrogen-β
PF5	Forward	5070	Continuum
PF6	Forward	5577	O (^{1}D-^{1}S)
PA1	Aft	2972	O (^{1}P-^{1}S)
PA2	Aft	2761	N_2 Vegard-Kaplan (0, 6)
PA3	Aft	3371	N_2 Second Positive (0, 0)
PA4	Aft	3914	N_2^+ First Negative (0, 0)
PA5	Aft	4861	Hydrogen-β
PA6	Aft	5070	Continuum

1. Dick, K.A., and Fastie, W.G. (1969) Up-down photometers for auroral profile studies, Applied Optics 8:2457.

The contribution from ground return is important at wavelengths longer than those of the ozone absorption region and must be considered in any nadir-viewing satellite system using wavelengths longer than about 3100 Å. Plots of column emission vs time, and vs altitude on ascent and descent are included for comparison with the results of model calculations.

2. DESCRIPTION OF THE PHOTOMETERS

Each photometer consisted of an interference filter, objective, field lens and an integrated photomultiplier detector system as shown in Figure 1. The interference filter and objective each had a clear aperture of 25 mm. The aperture of the field lens was 14 mm. It was located 127 mm behind the objective, resulting in a full field-of-view of 6 degrees. This gave a solid angle of 0.01 sr and throughput of 0.047 cm^2 sr.

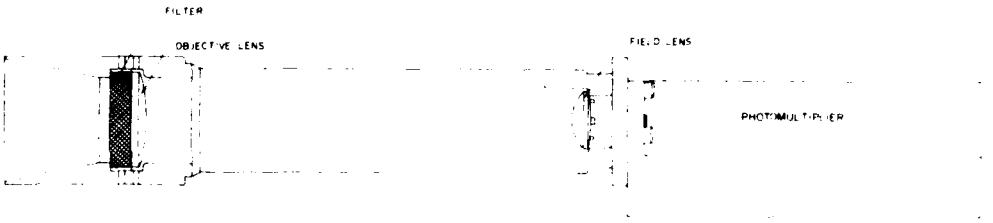

Figure 1. Schematic Diagram of Auroral-E Filter Photometers

The individual filter specifications are shown in Table 2. An additional specification which applied to all of the filters was attenuation of 5×10^{-6} (referred to the peak transmission) from 1800 Å to 8000 Å outside the passband of each filter.

The integrated photomultiplier detector systems were supplied by Epsilon Laboratories, Inc. Each system contained an EMR photomultiplier encapsulated with its own high-voltage power supply and pulse amplifier/discriminator. The three shortest wavelength photometers were equipped with EMR 510N-03-13 tubes having bi-alkali photocathodes and windows of 9741 UV transmitting glass. The other nine photometers were equipped with EMR 521N-01-CM channel multiplier tubes. These tubes also used bi-alkali photocathodes but had windows of 7056 glass.

The output from the detector systems was collected in counters, shifted every 100 msec and telemetered to ground stations.

Table 2. Filter Specifications

Photometer Designation	Central Wavelength (Å)	Peak Transmission (%)	Bandwidth (FWHM) (Å)
PF1	2761	10	45
PF2	3371	20	26
PF3	3912	5	28
PF4	4843	40	40
PF5	5070	40	40
PF6	5577	11	17
PA1	2972	10	40
PA2	2761	10	45
PA3	3371	20	26
PA4	3912	5	28
PA5	4879	40	40
PA6	5070	40	40

3. PHOTOMETRIC CALIBRATION FOR MEASUREMENTS OF THE ABSOLUTE INTENSITY OF A SPECTRAL EMISSION FEATURE

While filter photometers are extremely useful for rocket observations of aurora because of their simplicity, reliability and high throughput, they have the disadvantage of observation over a single wavelength band. As a result, knowledge of the spectral intensity distribution of the feature must be known to interpret the observed signal in terms of the absolute total intensity of the auroral feature.

The output of a photometer viewing any extended source may be given by

$$S = (10^6/6\pi) \int (R_\lambda(\lambda)\, A\, \Omega\, Q(\lambda)\, T(\lambda)\, d\lambda\,, \qquad (1)$$

where S is the signal in counts sec^{-1}, $R_\lambda(\lambda)$ is the spectral radiance of the source in rayleighs $Å^{-1}$, A is the area of the aperture in cm^2, Ω is the solid angle of the field in sr, $Q(\lambda)$ is the quantum efficiency of the detector, $T(\lambda)$ is the transmission of the system, which in a filter photometer is determined primarily by the filter and λ is the wavelength in Å. The integration extends over the wavelength range of the sensitivity of the instrument. The emission of the source is expressed in rayleighs because it is a convenient measure of apparent column emission.[2]

2. Chamberlain, J. W. (1961) Physics of the Aurora and Airglow, Academic Press, New York, p. 569.

One rayleigh equals an apparent column emission rate of 10^6 photons cm^{-2} column sec^{-1}.

It is convenient to combine the constant factors and instrumental parameters in Eq. (1) together to give

$$S = \int C(\lambda)\, R_\lambda(\lambda)\, d\lambda ,$$

where $C(\lambda) = (10^6/4\pi)\, A\, \Omega\, Q(\lambda)\, T(\lambda)$ and has units of counts $sec^{-1}\, R^{-1}$. The calibration function, $C(\lambda)$ may then be separated into a constant, C_o, and a wavelength dependent parameter, $\eta(\lambda)$, normalized so that $C(\lambda)$ equals C_o at λ_o, the wavelength of peak sensitivity. Thus $\eta(\lambda)$ becomes a relative instrumental response and C_o the absolute calibration constant. Eq. (1) then takes the form

$$S = C_o \int R_\lambda(\lambda)\, \eta(\lambda)\, d\lambda . \qquad (2)$$

The relative spectral response of each photometer, $\eta(\lambda)$, was determined by means of a continuous source followed by a monochromator arranged to illuminate a screen large enough to fill the photometer field-of-view as shown in Figure 2.

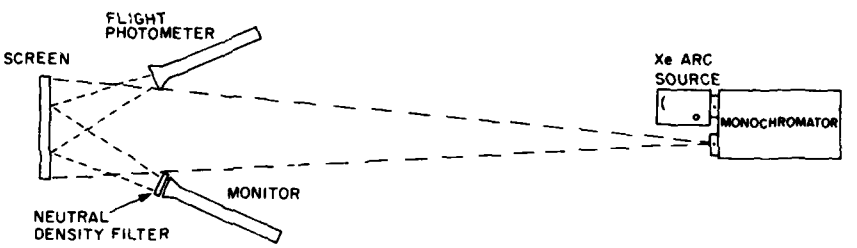

Figure 2. Optical Arrangement for Determining Relative Spectral Response

The monochromator was illuminated by a high-pressure xenon arc lamp. Because the bandwidth of the monochromator is narrow compared with the bandwidth of the photometers, the relative spectral responses were determined directly by dividing the photometer signals by the output of the monitor and normalizing the peak responses to unity. The monitor viewed the screen as shown in Figure 2. It consisted of a photometer assembly which lacked an interference filter, and measured variations in the radiance of the screen which were caused primarily by variations in the output of the xenon arc lamp.

The absolute calibration constant of each photometer, C_o, was determined by illuminating the screen directly with a calibrated standard lamp. The screen was coated with Eastman White Reflectance Coating to provide a calibrated Lambertian reflecting surface. The coating is composed of highly purified barium sulfate. It is completely non-self-radiating and is characterized by high stability and a nearly perfect reflecting surface. The lamp consisted of an EG&G 597-1, 1000 W quartz halogen lamp with the ANSI designation FEL. It is calibrated in terms of spectral irradiance at a distance of 0.5 m from the lamp. The calibration of EG&G is directly traceable to the National Bureau of Standards. The lamp was enclosed in an EG&G Model 597-3 lamp holder. This holder is based on the NBS design described in NBS Tech Note 594-2. A light-tight filter holder was used to mount neutral density filters at small but different angles so that multiple reflections from the filters were not directed onto the screen. A large black baffle was placed midway between the lamp holder and the screen to further control stray light.

The conversion of the spectral irradiance at a distance of 0.5 m in front of the lamp to the spectral radiance of the screen is given by

$$R_\lambda(\lambda) = 2.014 \times 10^8 \lambda\, r(\lambda)\, I_\lambda\, (0.5/d)^2 \qquad (3)$$

where $R_\lambda(\lambda)$ is the spectral radiance of the screen in units of rayleigh Å^{-1}, λ is the wavelength in Å, $r(\lambda)$ is the reflectivity of the screen, $I_\lambda(\lambda)$ is the spectral irradiance of the source at a distance of 0.5 m in W cm^{-2} nm^{-1}, and d is the distance from the source to the screen in m. The absolute calibration constant is calculated by rearranging Eq. (2),

$$C_o = S/[\int R_\lambda(\lambda)\, \eta(\lambda)\, d\lambda] \,. \qquad (4)$$

If the bandwidth of the photometer is narrow relative to the wavelength variation in the output of the standard lamp, as it is here, the integral in Eq. (4) may reduce to $R_\lambda(\lambda_o)\, W_{eq}$ where $R_\lambda(\lambda_o)$ is the spectral radiance of the screen at λ_o and W_{eq} is the equivalent width defined as $W_{ew} = \int \eta(\lambda)\, d\lambda$.

The absolute calibration factors and other calibration parameters are presented in Table 3. The relative spectral response for nine of the photometers is shown in Figures 3 through 11. The high-voltage supply section failed in three of the photometers prior to launch. The calibration data for these three were not processed.

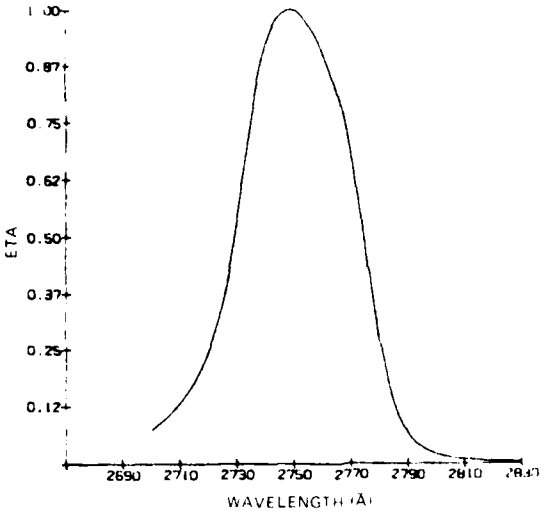

Figure 3. Relative Spectral Response of Photometer PF1

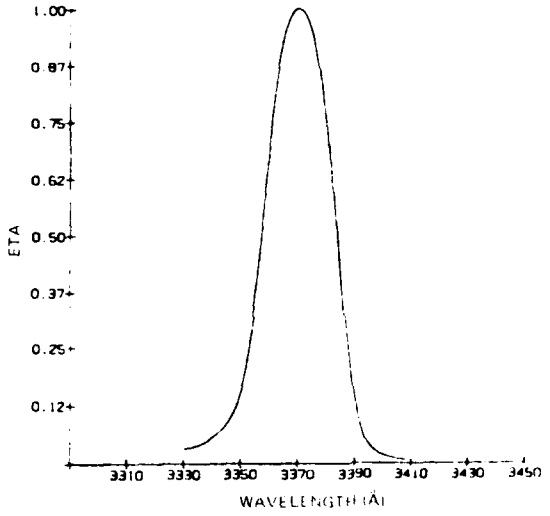

Figure 4. Relative Spectral Response of Photometer PF2

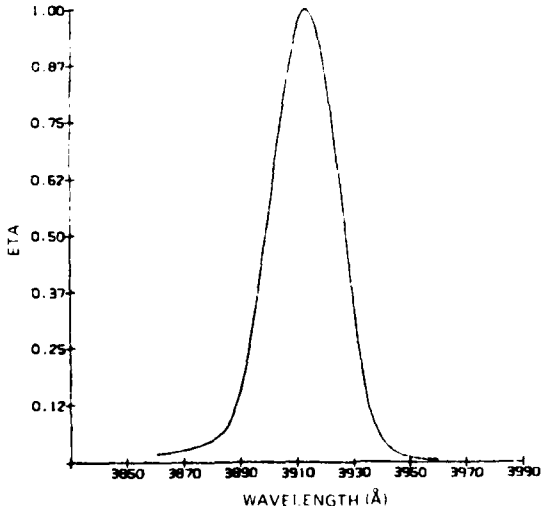

Figure 5. Relative Spectral Response of Photometer PF3

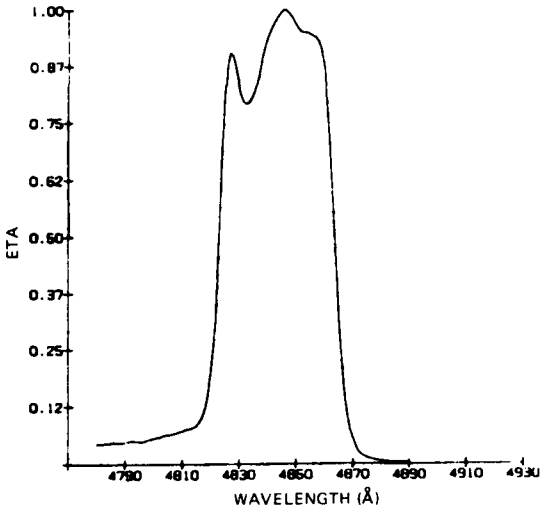

Figure 6. Relative Spectral Response of Photometer PF4

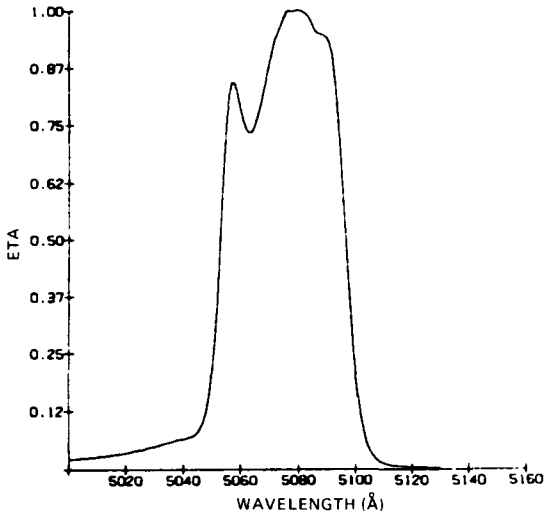

Figure 7. Relative Spectral Response of Photometer PF5

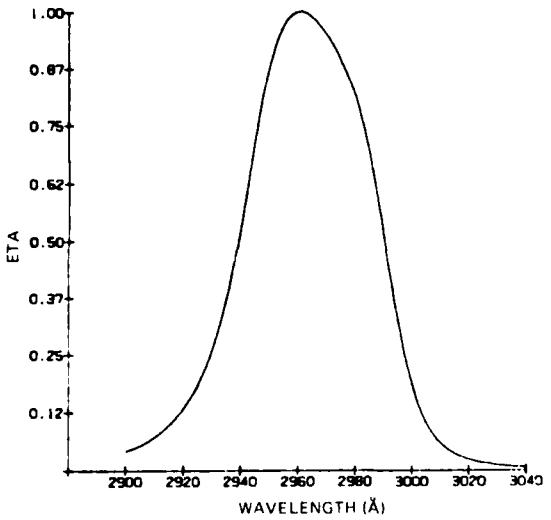

Figure 8. Relative Spectral Response of Photometer PA1

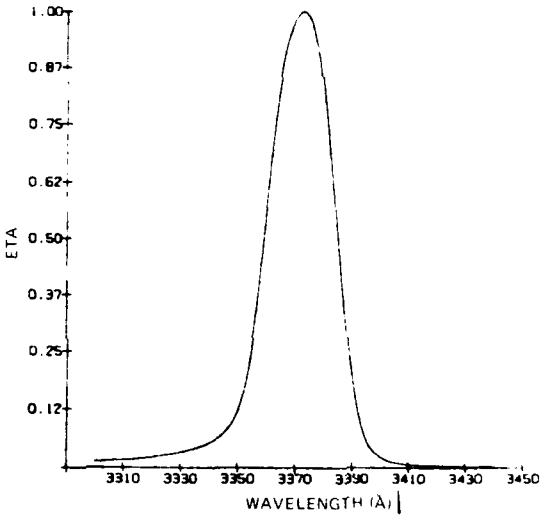

Figure 9. Relative Spectral Response of Photometer PA3

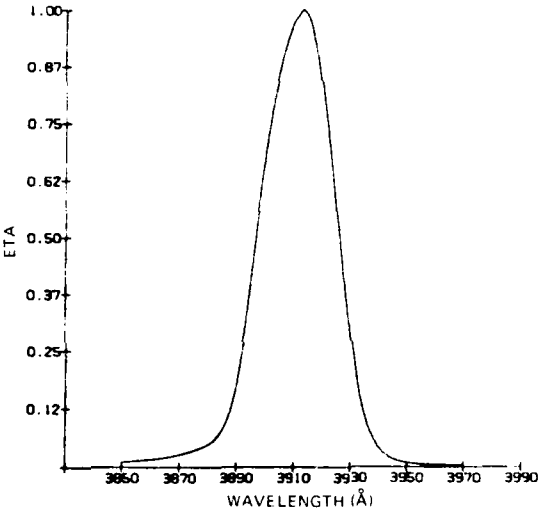

Figure 10. Relative Spectral Response of Photometer PA4

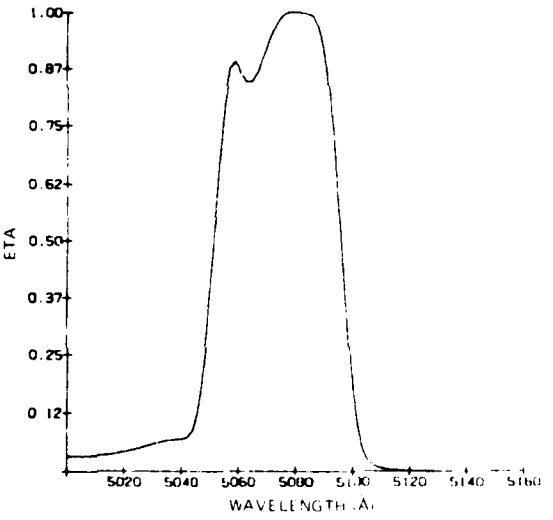

Figure 11. Relative Spectral Response of Photometer PA6

Table 3. Photometer Calibration Parameters

Photometer Designation	Spectral Feature	λ_o (Å)	W_{eq} (Å)	C_o (Cts R^{-1})	$C_o W_{eq}$ (Cts R^{-1} Å^{-1})
PF1	2761 Å	2749	48.3	5.2	252
PF2	3371 Å	3370	28.2	5.6	159
PF3	3914 Å	3913	30.1	1.69	50.8
PF4	4843 Å	4846	40.9	6.39	261
PF5	Continuum	5080	43.1	4.48	193
PA1	2972 Å	2961	54.5	9.0	489
PA3	3371 Å	3373	28.5	6.6	189
PA4	3914 Å	3913	31.0	1.49	46.3
PA6	Continuum	5079	45.0	5.73	258

The output of a photometer viewing emission from a single line is given by

$$S = C_o \, R_{line} \, \eta(\lambda_{line}) , \tag{5}$$

where R_{line} is the absolute intensity of the line in rayleighs, C_o is the absolute calibration constant for the photometer, and $\eta(\lambda_{line})$ is the relative spectral response of the photometer at the wavelength, λ_{line}, of the line emission.

For a photometer viewing a multiplet or a molecular band which consists of individual vibration-rotation lines, the signal is given by

$$S = C_o \, R_{band} \sum \beta_i \, \eta(\lambda_i) , \tag{6}$$

where R_{band} is the total intensity of the multiplet or the vibration-rotation band, β_i is the relative intensity which each line contributes to the total, and $\eta(\lambda_i)$ is the relative spectral response of the photometer at each of the lines. $\sum \beta_i \, \eta(\lambda_i)$ is known as the relative band response. It is the response of the photometer to the radiation which is distributed over the band relative to its response to radiation which is centered completely as a line at the wavelength of peak sensitivity, λ_o. The β_i's are determined by calculating a synthetic spectrum. They are normalized so that $\sum \beta_i = 1$.

For a photometer viewing a feature which has a continuous distribution of intensity, such as the strongly Doppler-broadened H_β line, the signal is given by

$$S = C_o \, R \int \beta_\lambda(\lambda) \, \eta(\lambda) \, d\lambda , \tag{7}$$

where $\beta_\lambda(\lambda)$ is the spectral distribution of intensity over the line. Here $\int\beta_\lambda(\lambda)$ is normalized to unity.

The validity of the calibration technique was corroborated by cross-calibrating two other Auroral-E instruments which had been previously calibrated by completely different techniques. One instrument was the airborne spectrometer flown by Jim Moore in the AFGL auroral observatory and calibrated by means of the AFGL C_{14} low-intensity source. This source has been intercalibrated with a number of other sources world-wide through the intercalibration program of the International Association of Geomagnetism and Aeronomy.[3]

The other instrument was the rocket spectrometer flown by Duane Paulsen. The spectrometer was calibrated in the AFGL VUV calibration facility described by Huffman et al.[4] The results of comparing the different calibration techniques showed agreement to within 10 percent and is within the experimental errors associated with the calibration techniques.

4. DESCRIPTION OF THE ROCKET LAUNCH

The rocket payload was launched in a northeasterly direction from the Poker Flats Research Range, Alaska (latitude: 65° 7'48" N; longitude: 147° 29'9" W) on 7 March 1981 at 0809 UT by a Taurus Orion rocket. This rocket, designated A13.030, was the first of four rockets launched in close succession as part of the AFGL Auroral-E program. It reached an apogee of 156 km.

Payload separation occurred at 69.0 sec (75.8 km), exposing the aft photometers. After this, the attitude control system (ACS) tilted the payload to approximately 45 degrees for nose cone ejection. The cone was ejected at 82.0 sec (90.8 km), exposing the forward photometers. After nose cone ejection, the ACS returned the payload to a vertical position for the duration of the flight. The ACS was set with wide limits so that it would cycle infrequently. The elevation of the vehicle and hence the direction of the photometer fields-of-view during flights is shown in Figure 12.

---

3. Torr, M. R., Espy, P. E., and Wraight, P. (1981) Intercalibration of Instrumentation Used in the Observation of Atmospheric Emissions: Second Progress Report 1981, Report No. CASS-101, Center for Atmospheric and Space Sciences, Utah State University, UMC 41, Logan, Utah 84322.

4. Huffman, R. E., LeBlanc, F. J., Larrabee, J. C., and Paulsen, D. E. (1980) Satellite vacuum ultraviolet and auroral observations, J. Geophys. Res. 85:2201.

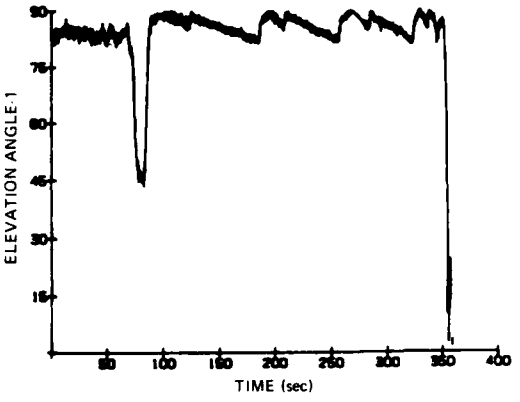

Figure 12. Elevation Angle of Rocket During Flight

5. RESULTS

5.1 N_2^+ 1st Negative (0,0) at 3914 Å

The bright emission at 3914 Å arises from the 0, 0 band of the N_2^+ 1N system. Emission from this system has long been used as a monitor of incident electron flux because of its direct proportionality to the ionization rate. The nitrogen ions which give rise to the N_2^+ 1N system are caused by simultaneous ionization and excitation of the N_2 molecule,[5]

$$N_2(X\ ^1\Sigma_g^+) + M \rightarrow N_2^+(B\ ^2\Sigma_u^+) + M + e\ , \tag{8}$$

where M may be an exciting electron or proton. This initial excitation is followed by decay of the B state to the ground state of the ion with emission of the 1st negative system:

$$N_2^+(B\ ^2\Sigma_u^+) \rightarrow N_2^+(X\ ^2\Sigma_g^+) + h\nu_{1N}\ . \tag{9}$$

The decay is optically allowed and occurs rapidly. Shemansky and Broadfoot[6] calculate a lifetime for the B state as 9×10^{-8} sec; thus the transition occurs without collisional quenching of the upper state at altitudes associated with the

5. Bates, D. R. (1949) The intensity distribution in the nitrogen band systems emitted from the earth's upper atmosphere, Proc. Roy. Soc. (London), Ser. A. 196:217.

6. Shemansky, D. E., and Broadfoot, A. L. (1971) Excitation of N_2 and N_2^+ systems by electrons. I: Absolute transition probabilities, J. Quant. Spectrosc. Radiat. Transfer 11:1385.

auroral-E layer. The peak in the cross-section for this reaction occurs about 100 eV for M as electrons.[7]

As the transition belongs to Hund's case (b), P and R branches are formed. The wavelengths of the lines in these branches were determined by using the spectroscopic constants given by Huber and Herzberg,[8] ignoring ρ-type doubling. The relative intensities of the lines within the band is given by the product of the line strengths and the Boltzman factor, and, because N_2 is a homonuclear diatomic molecule, a statistical weight due to the effect of nuclear spin. The line strengths were taken from the compilation of line strengths given by Kovacs.[9] The Boltzman factor was calculated using the rotational constants of the ground state of the neutral molecule because, owing to the smallness of the electron mass, no significant change in the angular momentum of the system is produced as it is excited by electron impact. Therefore the distribution of molecules over the different levels in the upper electronic state is practically the same as the ground state.[10] The resulting synthetic spectra are shown in Figure 13 at neutral temperatures ranging from 200°K to 1000°K. The broadening of the band as the higher rotational states are populated at higher temperatures is clearly shown.

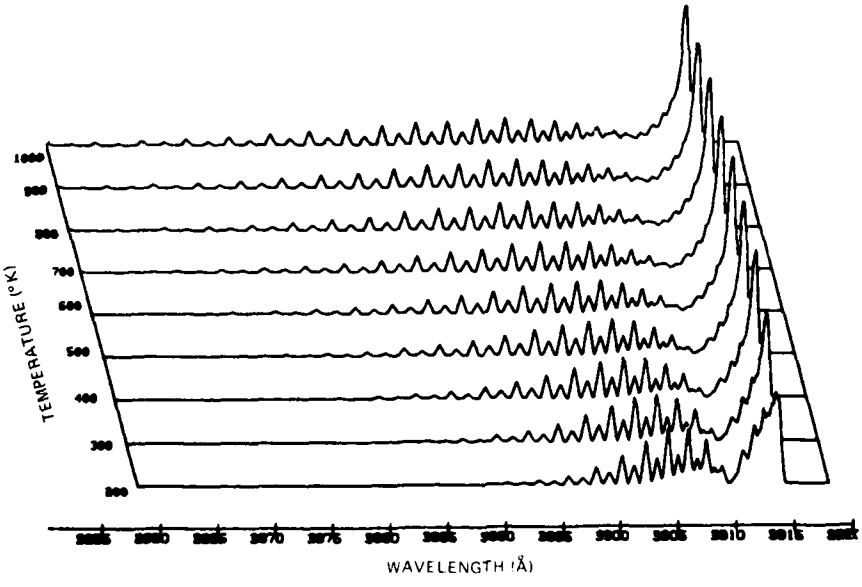

Figure 13. Synthetic Spectra of N_2^+ 1N(0, 0) at 3914 Å at Temperatures From 200°K to 1000°K

(Due to the large number of references cited above, they will not be listed here. See References, page 59.)

The band was observed by upward-viewing photometer PF3 and downward-viewing photometer PA4. The relative band response of N_2^+ 1NG(0, 0) with photometers PF3 and PA4 is shown in Figures 14 and 15. The relative band response, and therefore the sensitivity of the photometer, drops as the neutral temperature rises.

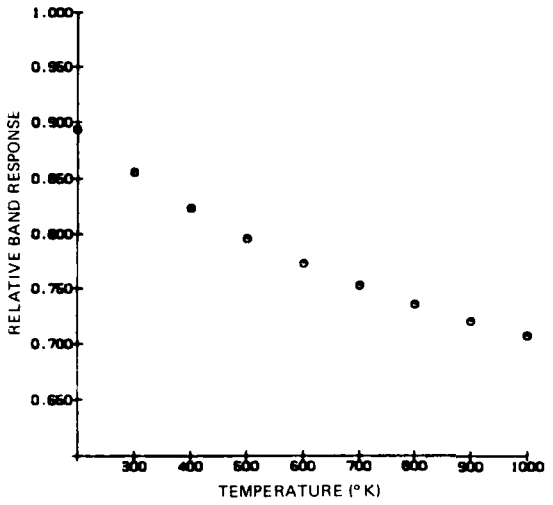

Figure 14. Relative Band Response of N_2^+ 1N(0, 0) and Photometer PF3 at Neutral Temperatures Between 200°K and 1000°K

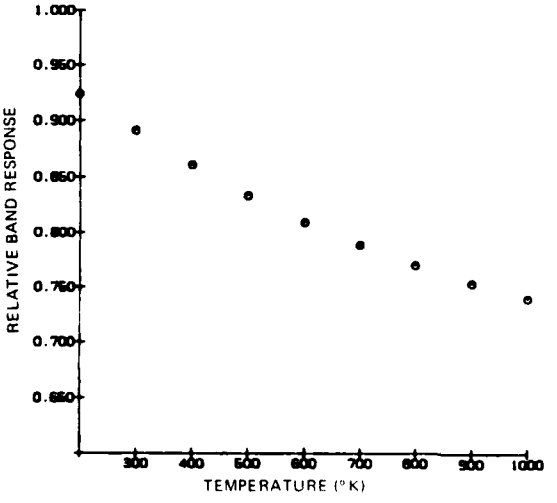

Figure 15. Relative Band Response of N_2^+ 1N(0, 0) and Photometer PA4 at Neutral Temperatures Between 200°K and 1000°K

Unfortunately photometer PA4 suffered from sporadic high voltage failure as shown in Figure 16, which plots the raw signal and the high-voltage monitor vs time. Despite sporadic high-voltage failure, it can be seen that there are periods of useful data.

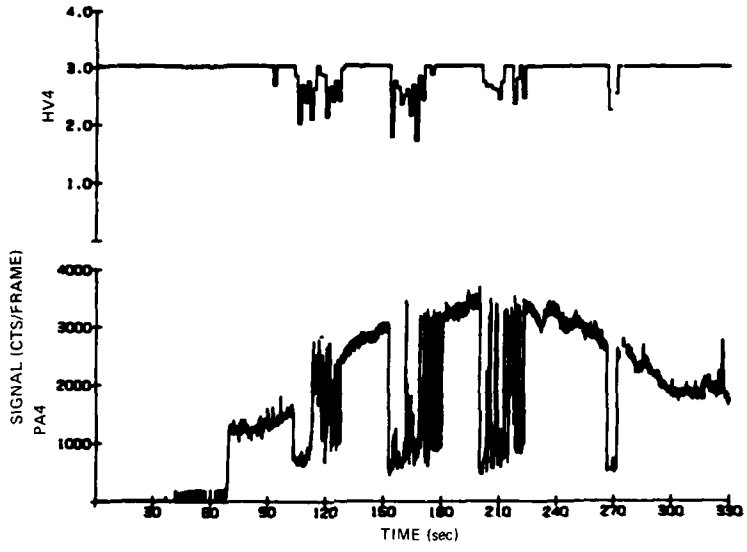

Figure 16. PA4 Signal and High Voltage Monitor Outputs vs Time

The apparent column emission of N_2^+ 1N(0, 0) as measured by the upward-viewing photometer PF3 is plotted in Figure 17 vs time and in Figures 18 and 19 vs altitude for the upleg and downleg portions of the flight respectively. The same series of plots for the downward-viewing photometer PA4 is given in Figures 20, 21 and 22. The signal from photometer PA4 below about 100 km is due to ground return. This is caused predominantly by auroral radiation from the entire sky which is reflected from the snow-covered Alaskan terrain below the rocket. The amount reflected from the terrain brightened from about 1000 R at the beginning of the data taking period to as much as 1500 R at the end of the flight. Plots of the sum of the signals from the upward-viewing and downward-viewing photometers are useful to separate altitude variations from time variations and also to simulate the signal which would be observed from a satellite system looking down at the auroral-E layer from above. The sum of the up and down signals is plotted as a

function of time in Figure 23, and as functions of altitude for the upleg and downleg portions of the flight in Figures 24 and 25 respectively.

Although gaps in the data are left where the high-voltage power supply failed on the down-viewing photometer, the data still are adequate to show a general brightening from about 2500 R at the beginning of the data taking period to a peak radiance of about 3000 R at about 200 sec after launch. The data from the downleg portion of the flight shows small pulsations with a period of approximately 20 seconds. It should be pointed out that these sums include the effect of ground return of approximately 1000 R. The total column emission from the atmosphere alone, not including the contribution from the ground return, was about 1200 R.

5.2 N_2 2nd Positive (0,0) at 3371 Å

The emission at 3371 Å arises from the 0, 0 band of the N^2 and positive system. This system is excited by electron impact of ground state nitrogen to the C state in the triplet system:

$$N_2(X\ ^1\Sigma_g^+) + e \rightarrow N_2(C\ ^3\Pi_u) + e\ , \tag{10}$$

followed by decay of the C state to the B state with emission of the 2P system,

$$N_2(C\ ^3\Pi_u) \rightarrow N_2(B\ ^3\Pi_g) + h\nu_{2P}\ . \tag{11}$$

While the peak in the cross-section for excitation of the N_2^+ 1N system occurs about 100 eV, the cross-section for the reaction given by Eq. (10) is strongly peaked about 15 eV. A value of 0.38×10^{-16} cm^2 has been measured by Shemansky and Broadfoot.[11]

The decay is optically allowed and occurs rapidly with a lifetime given as 9×10^{-8} sec.[6] Therefore, like the N_2^+ 1N system, collisional quenching of the C state is negligibly small at altitudes associated with the auroral-E layer.

---

11. Shemansky, D. E., and Broadfoot, A. L. (1971) Excitation of N_2 and N_2^+ systems by electrons, II: Excitation cross-sections and N_2 1PG low pressure afterglow, J. Quant. Spectrosc. Radiat. Transfer 11:1401.

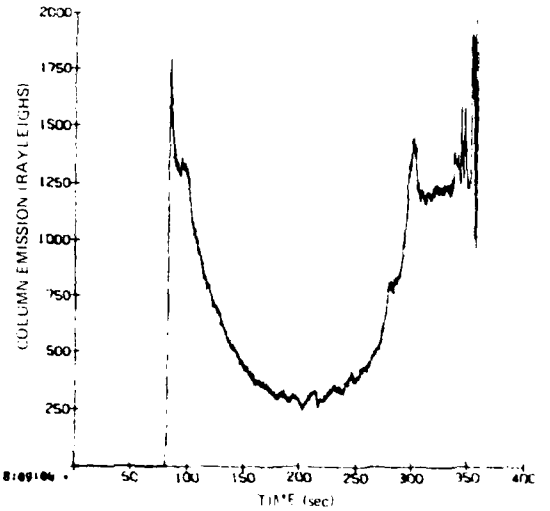

Figure 17. Apparent Column Emission of N_2^+ 1N(0, 0) vs Time From Photometer PF3

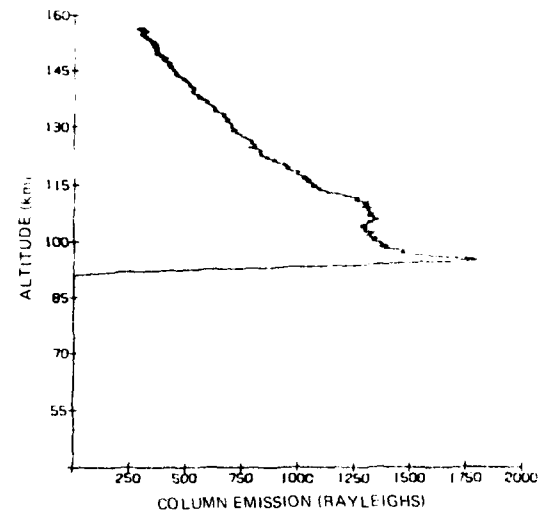

Figure 18. Apparent Column Emission of N_2^+ 1N(0, 0) vs Altitude From Photometer PF3 (Upleg)

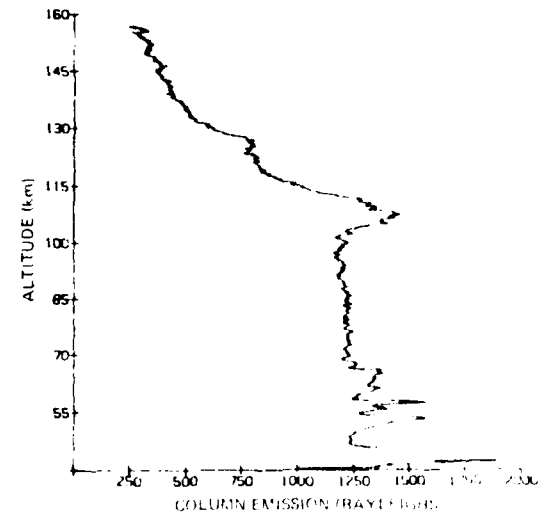

Figure 19. Apparent Column Emission of N_2^+ 1N(0, 0) vs Altitude From Photometer PF3 (Downleg)

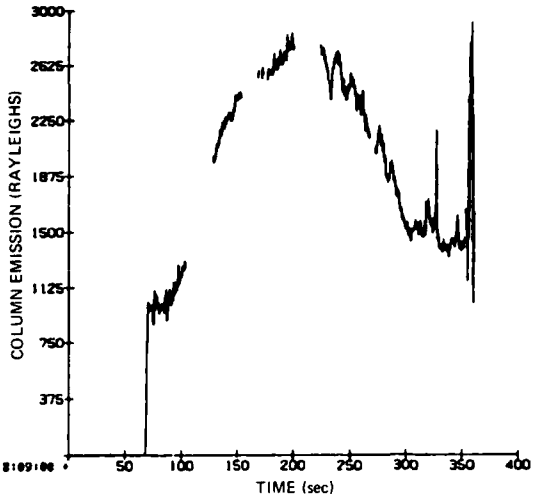

Figure 20. Apparent Column Emission of N_2^+ 1N(0, 0) vs Time From Photometer PA4

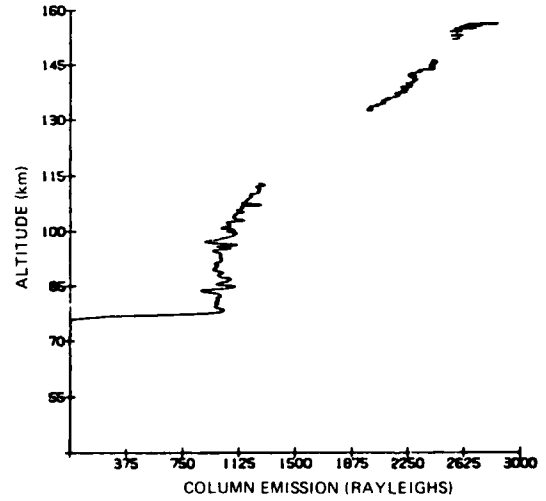

Figure 21. Apparent Column Emission of N_2^+ 1N(0, 0) vs Altitude From Photometer PA4 (Upleg)

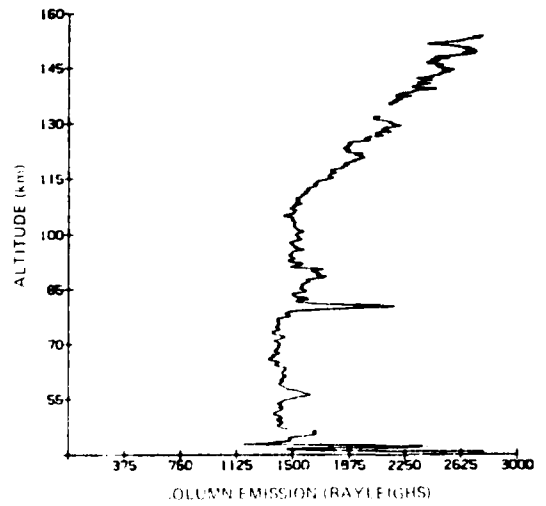

Figure 22. Apparent Column Emission of N_2^+ 1N(0, 0) vs Altitude From Photometer PA4 (Downleg)

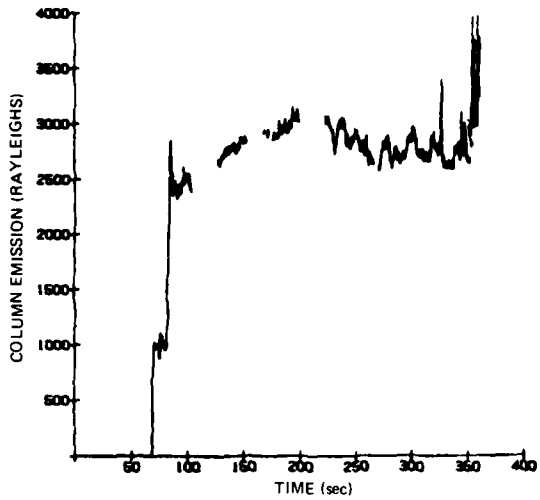

Figure 23. Sum of Apparent Column Emission of N_2^+ 1N(0, 0) vs Time From Photometers PF3 and PA4

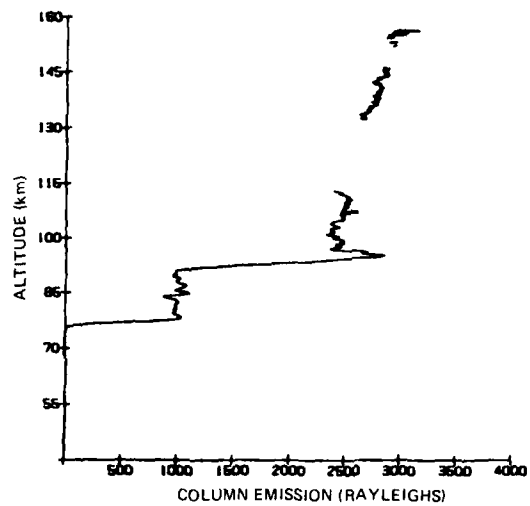

Figure 24. Sum of Apparent Column Emission of N_2^+ 1N(0, 0) vs Altitude From Photometers PF3 and PF4 (Upleg)

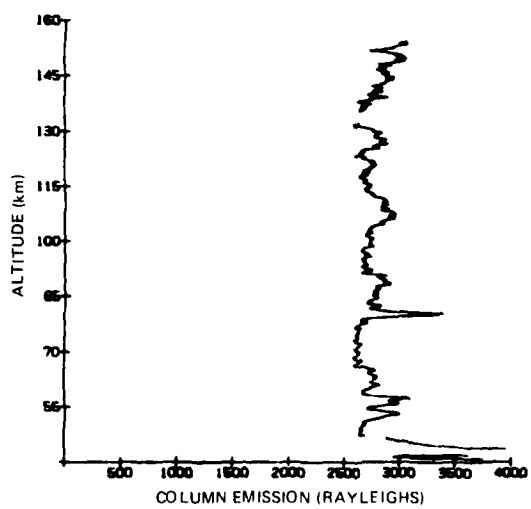

Figure 25. Sum of Apparent Column Emission of N_2^+ 1N(0, 0) vs Altitude From Photometers PF3 and PA4 (Downleg)

The transition in Eq. (11) belongs to Hund's case (a), each sub-band consisting of a strong P branch, a strong R branch, and, except for $^3\Pi_o - {}^3\Pi_o$, a weak Q branch. In calculating the synthetic spectrum we have included the effect of multiplet splitting but neglected Λ-type doubling. Since we neglected Λ-type doubling, we did not have to consider the intensity alternation usually associated with nuclear spin in homonuclear diatomics. This is because the unresolved doublet consists of both the strong and weak line in the pair. The molecular constants were taken from the compilation of Huber and Herzberg,[8] and the line strengths from Kovacs.[9] As in the previous case, ground state molecular constants were used in computing the Boltzman factor. The resulting synthetic spectra are shown in Figure 26. The three separate branches are clearly shown: the P branch forming the band head, the R branch which is shaded strongly toward shorter wavelengths and shows the rotational structure and the weak Q branch which is evident between the P and R branches.

The emission from this band was observed by upward-viewing photometer PF2 and downward-viewing photometer PA3. The relative band responses of N_2 2PG(0, 0) with these photometers are shown in Figures 27 and 28.

The apparent column emission of N_2 2P(0, 0) as measured by the upward-viewing photometer PF2 is plotted in Figure 29 vs time and in Figures 30 and 31 vs altitude for the upleg and downleg portions of the flight. The same series of plots for the downward-viewing photometer PA3 is given in Figures 32, 33 and 34.

As in the case of the 3914 Å band, there is significant radiation observed by the downward-viewing photometer which is attributable to ground return. Interpreting radiation observed when the rocket was looking downward from below 100 km as due to ground return, the amount brightened from about 310 R at the beginning of the data-taking period to as much as 460 R at about 300 sec after launch.

Plots of the sum of the signals from the upward-viewing and downward-viewing photometers are given as a function of time in Figure 35, and as functions of altitude for the upleg and downleg portions of the flight in Figures 36 and 37, respectively. The summed signals clearly show that the structure which appears on the individual upward-viewing and downward-viewing altitude plots is a variation in the total intensity of the aurora during the time of the flight and not a true altitude variation.

The total radiance which would be observed from a satellite system looking down at the aurora would have been about 925 R. The column emission from the atmosphere alone was 625 R.

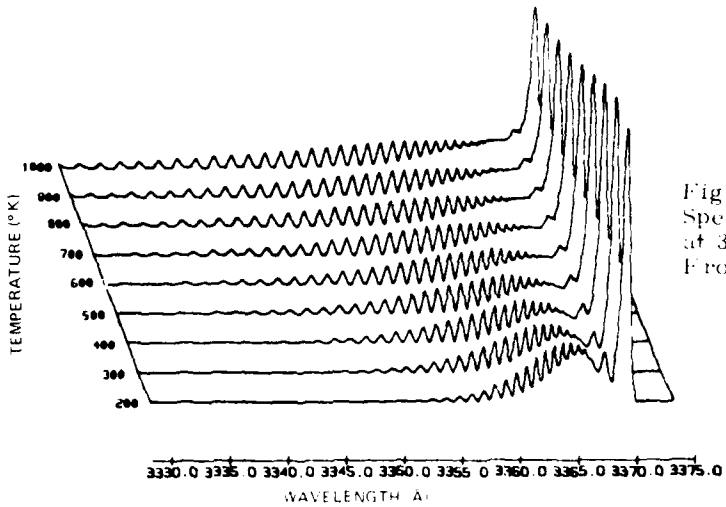

Figure 26. Synthetic Spectra of N_2 2P(0, 0) at 3371 Å at Temperatures From 200°K to 1000°K

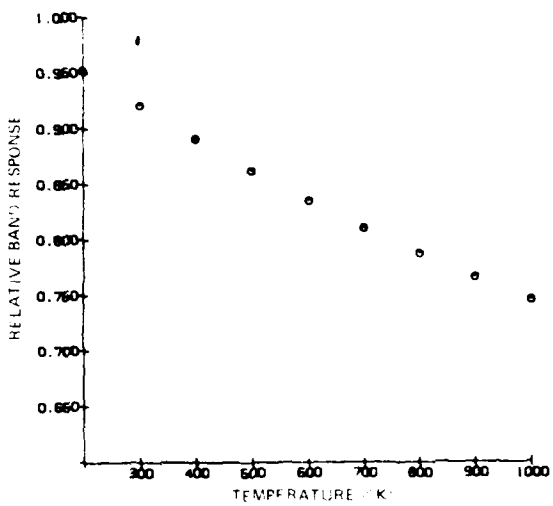

Figure 27. Relative Band Response of N_2 2P(0, 0) and Photometer PF2 at Neutral Temperatures Between 200°K and 1000°K

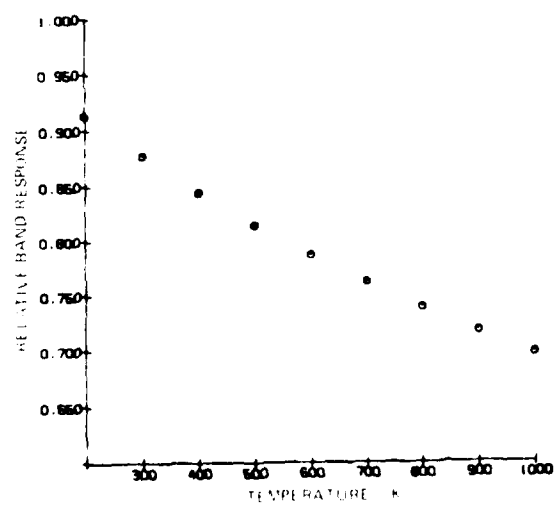

Figure 28. Relative Band Response of N_2 2P(0, 0) and Photometer PA3 at Neutral Temperatures Between 200°K and 1000°K

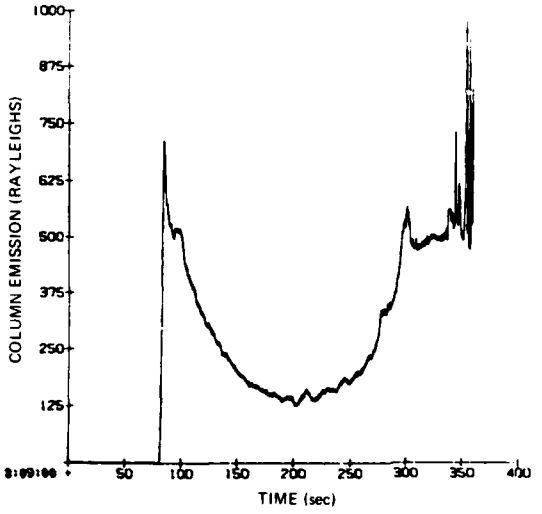

Figure 29. Apparent Column Emission of N_2 2P(0, 0) vs Time From Photometer PF2

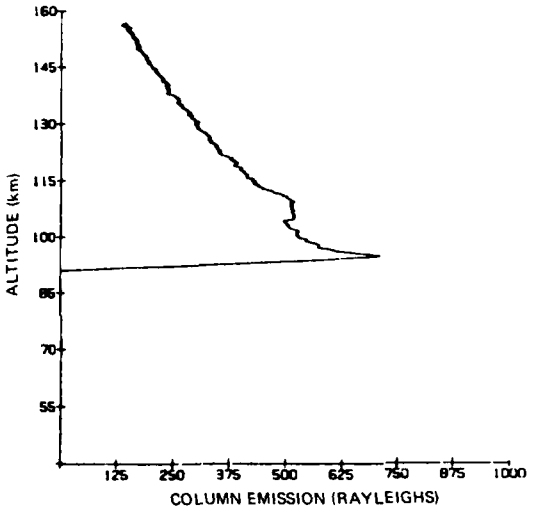

Figure 30. Apparent Column Emission of N_2 2P(0, 0) vs Altitude From Photometer PF2 (Upleg)

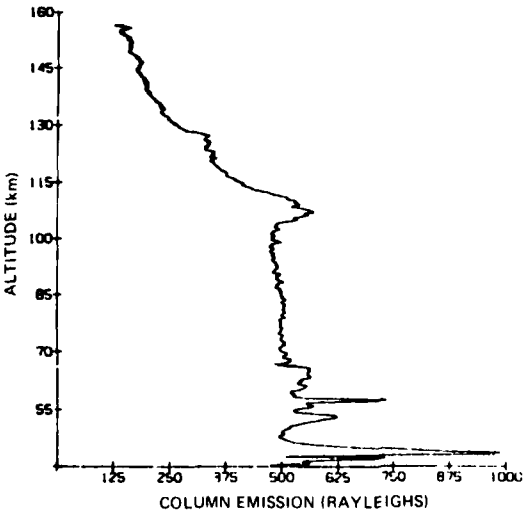

Figure 31. Apparent Column Emission of N_2 2P(0, 0) vs Altitude From Photometer PF2 (Downleg)

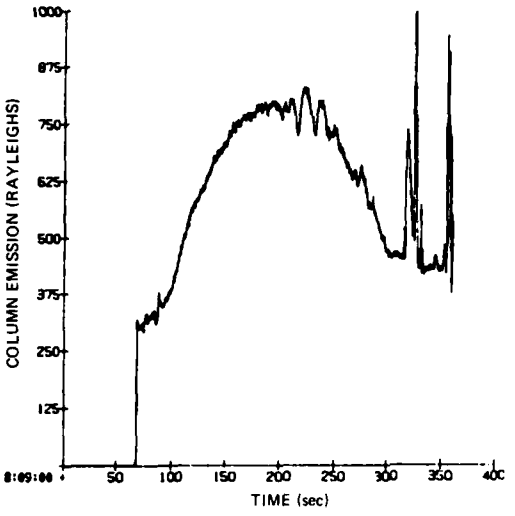

Figure 32. Apparent Column Emission of N_2 2P(0, 0) vs Time From Photometer PA3

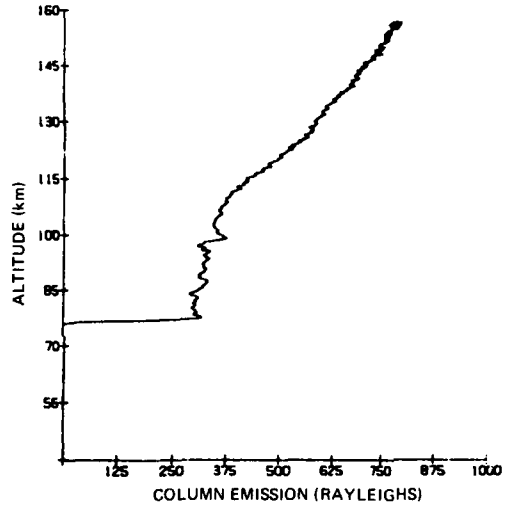

Figure 33. Apparent Column Emission of N_2 2P(0, 0) vs Altitude From Photometer PA3 (Upleg)

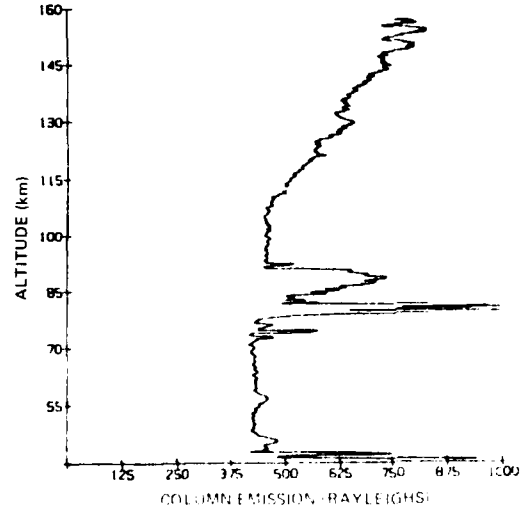

Figure 34. Apparent Column Emission of N_2 2P(0, 0) vs Altitude From Photometer PA4 (Downleg)

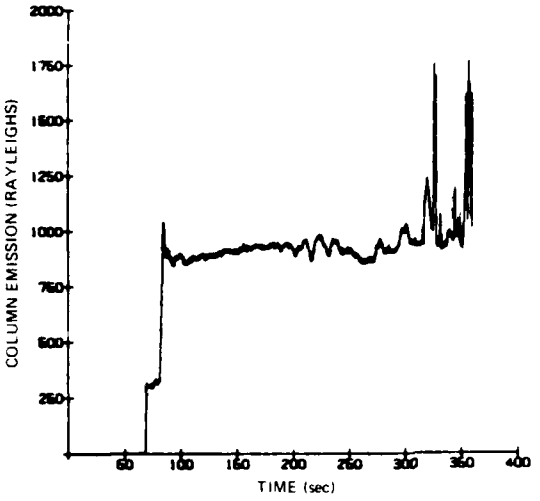

Figure 35. Sum of Apparent Column Emission of N_2 2P(0, 0) vs Time From Photometers PF2 and PA3

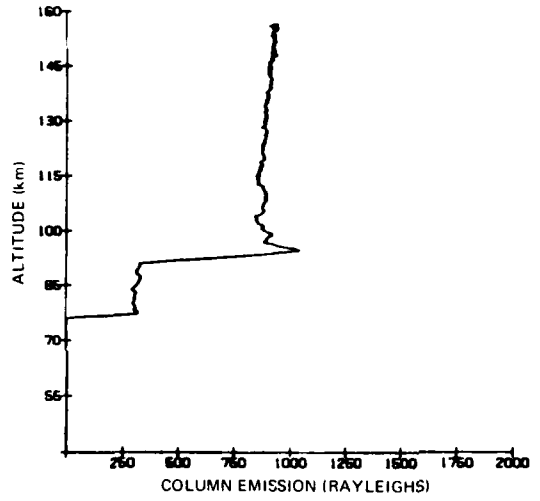

Figure 36. Sum of Apparent Column Emission of N_2 2P(0, 0) vs Altitude From Photometers PF2 and PA3 (Upleg)

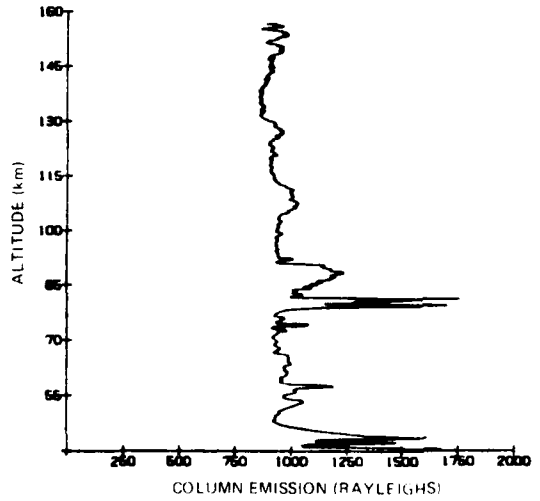

Figure 37. Sum of Apparent Column Emission of N_2 2P(0, 0) vs Altitude From Photometers PF2 and PA3 (Downleg)

5.3 N_2 Vegard-Kaplan (0,6) at 2761 Å

The N_2 Vegard-Kaplan bands are produced by transitions from the lowest term in the triplet system to the singlet ground state,

$$N_2(A\ ^3\Sigma_u^+) \rightarrow N_2(X\ ^1\Sigma_g^+) + h\nu_{VK} . \qquad (12)$$

The production of the $A\ ^3\Sigma_g^+$ state is dominated by cascading from upper levels in the triplet system which are produced by electron impact. The triplet state with the greatest production cross-section is the C state. The C state cascades to the B state producing the 2nd positive system discussed earlier, and the B state cascades in turn to the A state producing the 1st positive system. A full set of equations describing the cascading processes is given by Cartwright et al.[12]

The $A\ ^3\Sigma_u^+ - X\ ^1\Sigma_g^+$ transition is an electric dipole transition although "forbidden" by the difference in total electron spin between the two states. As the A state is a metastable state, quenching becomes an important loss process. A lifetime of ~2 sec has been measured by Shemansky.[13] Thie lifetime corresponds to a quenching height of about 145 km,[14] the quenching height being defined as the height at which the emission rate is reduced to one-half of its unquenched value. Above this height the quenching rapidly becomes negligible, while below, its effects are severe.

The $A\ ^3\Sigma_u^+$ state deviates from Hund's case (b) because the triplet levels are split and the levels separable. The slight splitting between levels with different J and equal K is due to interactions resulting from vibration and rotation, along with a large contribution from electron spin-spin interaction.[15, 16] This splitting results in four branches, which using the nomenclature of Herzberg,[10] are designated R, ^RQ, ^PQ and P. The values of the molecular constants used to calculate the positions of the lines were taken from the compilation of Huber and Herzberg.[8]

The intensities are given by the product of the line strengths, the Boltzman factor and, again, as this is a homonuclear diatomic molecule, a statistical weight due to the interaction of nuclear spin with the total electron spin. The line strengths were taken from Shemansky,[13] and the Boltzman factor was calculated using the molecular constants of the ground state for the reasons given earlier.

The synthetic spectra at temperatures ranging from 200°K to 1000°K is shown in Figure 38. The band is broader than the N_2^+ 1st negative or the N_2 2nd positive bands, and therefore, the relative band response of the photometer would be expected to be strongly dependent on the temperature of the neutral atmosphere.

(Due to the large number of references cited above, they will not be listed here. See References, page 59.)

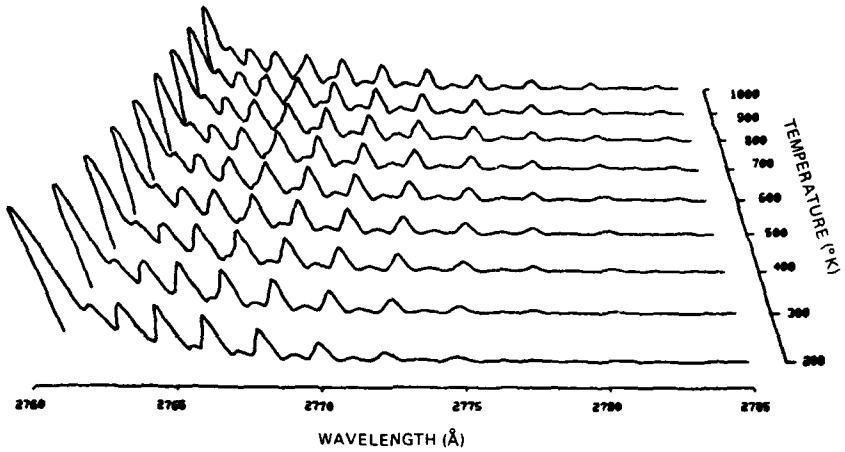

Figure 38. Synthetic Spectra of N_2 VK(0, 6) at 2761 Å at Temperatures From 200°K to 1000°K

The emission from the band was observed by the upward-viewing photometer PF1. The high-voltage power supply failed prior to launch in the downward-viewing photometer planned to measure this radiation. The relative band reponse of the band with the upward-viewing photometer is shown in Figure 39. The strong variation of the relative band response, and hence the sensitivity of the instrument, varies from a high of 0.8 for a neutral atmosphere temperature of 200°K to only 0.5 for a neutral atmosphere of 1000°K.

The apparent column emission of the N_2 VK(0, 6) is given vs time in Figure 40, and vs altitude on upleg and downleg in Figures 41 and 42. The apparent column emission varies from a maximum of about 160 R looking upward at 85 km to about 75 R at the apogee of 156 km. The fall off of the intensity with altitude is noticeably less than that of either the N_2^+ 1st negative or the N_2 2nd positive bands, indicating proportionately less production at lower altitudes. This is consistent with a higher susceptability to quenching. The continued increase in the observed intensity below 100 km on downleg is, however, perplexing.

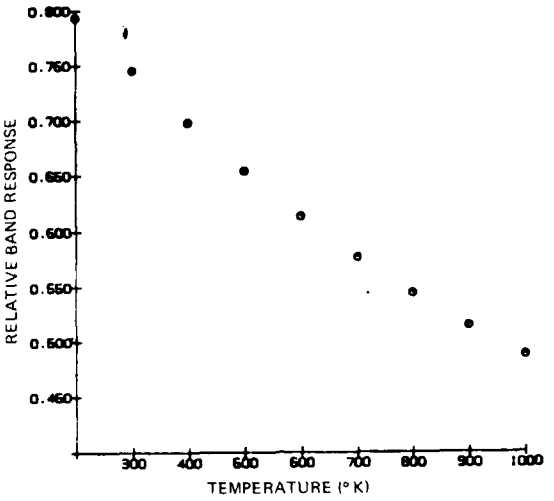

Figure 39. Relative Band Response of N_2 VK(0, 6) and Photometer PF1 at Neutral Temperatures Between 200°K and 1000°K

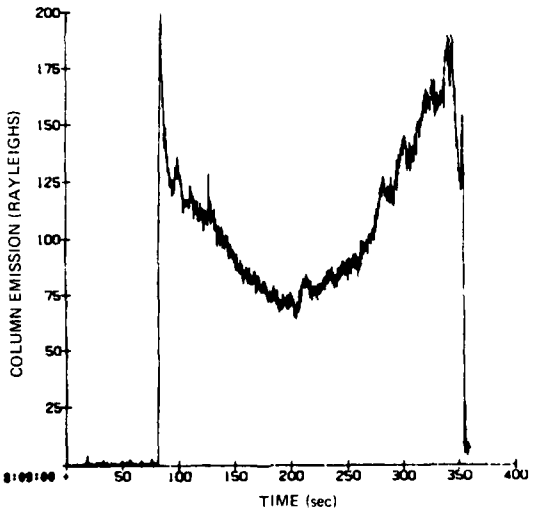

Figure 40. Apparent Column Emission of N_2 VK(0, 6) vs Time From Photometer PF1

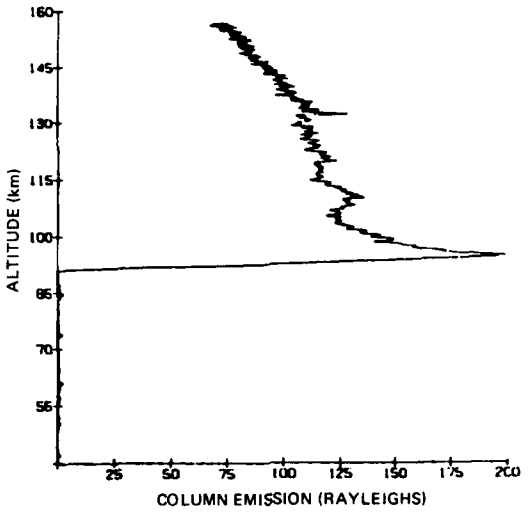

Figure 41. Apparent Column Emission of N_2 VK(0, 6) vs Altitude From Photometer PF1 (Upleg)

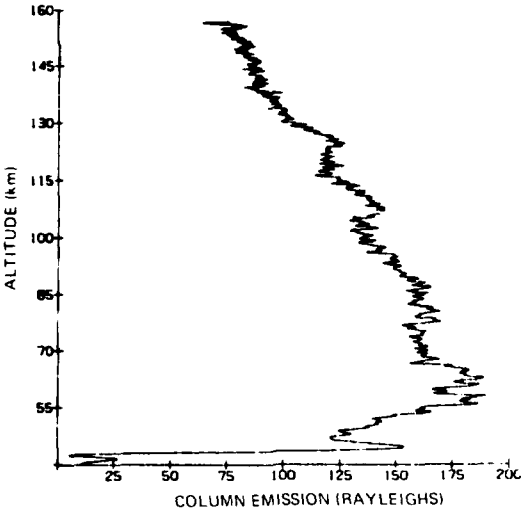

Figure 42. Apparent Column Emission of N_2 VK(0, 6) vs Altitude From Photometer PF1 (Downleg)

5.4 OI ($^1S - {}^3P$) at 2972 Å

Like the "green line" at 5577 Å, the emission at 2972 Å results from decay of the ^1S state of atomic oxygen. While the emission at 5577 Å results from $^1D - {}^1S$ transition, the emission at 2972 Å is produced by decay of the ^1S state to the ^3P ground state. The ratio of the intensity of 2972 Å to that at 5577 Å is given by the theoretical transition probabilities as 0.06.[14] The great advantage of using emission at 2972 Å instead of 5577 Å in a system which looks down at the earth is that the emission at 2972 Å which is directed downward is absorbed by ozone in the stratosphere and hence the observed signal has no contribution due to ground return. This is clearly evident in the downward-viewing photometer signals in Figure 43 which shows a plot of the signal vs time and in Figures 44 and 45 which plot the signal vs altitude for the upleg and downleg portions of the flight. In contrast to the longer wavelength photometers, there is negligible signal observed below about 85 km.

While the 2972 Å line does not have a contribution due to ground return, it is not as bright as the 5577 Å line, and in addition the signal is contaminated by other bands in the two molecular nitrogen systems discussed earlier. The nitrogen bands which contribute to the signal are the 2, 0; 3, 1 and 4, 3 bands of the 2nd positive system and the 0, 7 and 0, 8 bands in the Vegard-Kaplan system. The amount of this contribution is evaluated and assessed by using the data from the photometers which measured the intensity of the 2nd positive system in the 0, 0 band at 3371 Å, and the Vegard-Kaplan system in the 0, 6 band at 2761 Å.

The total signal observed by photometer PA1 at height, z, may be considered as the sum of the contributions from atomic oxygen and the molecular niteogen bands, that is,

$$S(PA1, z) = [S(2972;z) + S(2P;2, 0;z) + S(2P;3, 1;z) + S(2P;4, 3;z) + S(VK;0, 7;z) + S(VK;1, 8;z)] . \quad (12)$$

Here S(2972;z) refers to that part of the signal due to the 2972 Å emission and is given by

$$S(2972;z) = C_o(PA1)\, R(2972;z)\, \eta(PA1, 2972) . \quad (13)$$

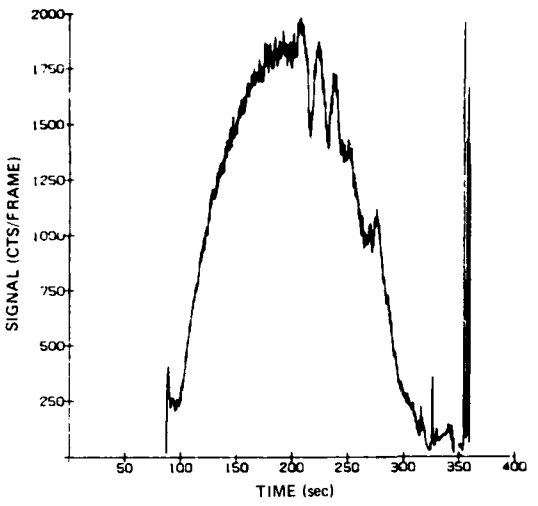

Figure 43. Signal From Photometer PA1 vs Time

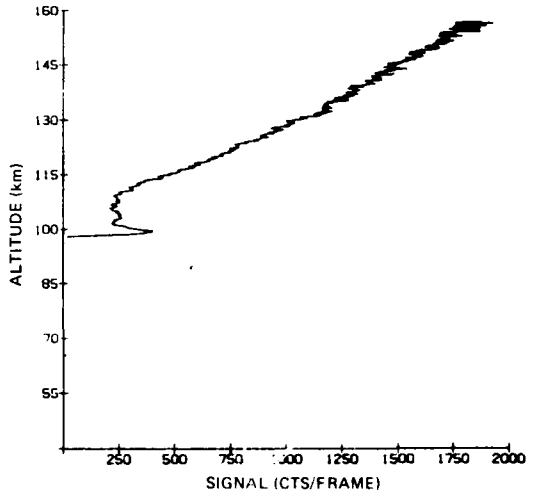

Figure 44. Signal From Photometer PA1 vs Altitude (Upleg)

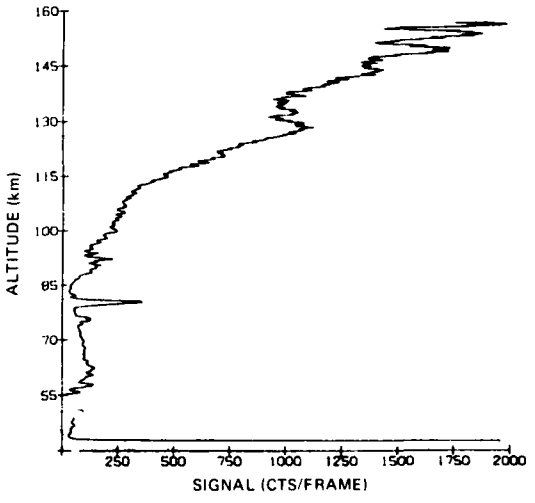

Figure 45. Signal From Photometer PA1 vs Altitude (Downleg)

The contribution to the signal from the molecular bands are of the form

$$S(2P;2,0;z) = C_o(PA1)\ R(2P;2,0;z) \sum_J \beta_J(2P;2,0)\ \eta(PA1;\lambda_J(2P;2,0)) , \quad (14)$$

where $\eta(PA1;\lambda_J(2P;2,0))$ refers to the relative spectral response of photometer PA1 at the wavelengths of the lines in the 2, 0 band of the 2nd positive system. The β's are normalized so that $\sum_J \beta_J = 1$.

The β's are calculated by means of synthetic spectra which are calculated as described earlier for the other bands in the systems. C_o and $\eta(\lambda)$ are determined by the calibration procedure. The R's are determined by using the signals in the other photometer channels which measured the intensity due to 2nd positive and Vegard-Kaplan emission, and the relative intensities of the bands taken from the tables of predicted relative intensities of bands in an electron aurora by Vallance Jones.[14] The values of relative intensity applicable to this work are reproduced in Table 4.

Table 4. Predicted-Relative Intensities in an Electron Aurora (see Reference 14)

System; Band	Wavelength Origin (Å)	Relative Intensity (5577 Å = 100)
2P; 0, 0	3371	30.68
2P; 2, 0	2976	1.88
2P; 3, 1	2961	1.04
2P; 4, 3	2952	0.40
2P; Total System		113
VK; 0, 6	2761.5	2.88
VK; 0, 7	2936.4	2.72
VK; 1, 8	2997.7	1.68
VK; Total System		55

The radiances of the 2,0; 3,1 and 4,3 bands of the 2nd positive system are found by correcting the observed radiance of the 0,0 band for ground return and multiplying by the predicted intensity ratios. The portion of the PA1 signal attributable to these bands is plotted vs time in Figures 46-48, and vs altitude for the upleg and downleg portions of the flight in Figures 49-54.

The radiances of the 0,7 and 1,8 bands of the Vegard-Kaplan system have to be inferred from the column emission of the 0,6 band as measured by the upward-viewing photometer PF1, because the high-voltage power supply of the downward-viewing photometer PA2 failed. Since there is no contribution from ground return at these wavelengths, the radiance looking down may be given by

$$R_{dn}(VK;0,6;z) = R_{100-156}(VK;0,6) - R_{up}(VK;0,6;z) ,$$

where $R_{dn}(VK;0,6;z)$ is the apparent column emission looking down, $R_{100-156}(VK;0,6)$ is the difference in radiance observed by the upward-viewing photometer PF1 between 100 km and the apogee of 156 km, and $R_{up}(VK;0,6;z)$ is the measured radiance as a function of altitude, z, as shown in Figures 40-42. Multiplying $R_{dn}(VK;0,6;z)$ by the predicted intensity ratios gives the radiance due to the 0,7 and 1,8 bands. The portion of the PA1 signal attributable to these bands is plotted vs time in Figures 55 and 56, and vs altitude for the upleg and downleg portions of the flight in Figures 57-60.

Finally, the values for the contribution to the PA1 signal may be substituted into Eq. (12), and the equation solved for S(2972;z). This function may then be used to solve for R(2972,z) by using Eq. (13). The results are shown in Figures 61 which plots the emission vs time, and in Figures 62 and 63 which plot the emission vs altitude on upleg and downleg, respectively. The radiance at apogee, looking down, represents 220 R of 0 $^1S - ^3P$ emission. This is the equivalent of 3.6 kR of 5577 Å emission. The proportion of the signal from the various emissions is shown at apogee in Table 5. About half of the signal from photometer PA1 is attributable to the atomic oxygen emission, the remainder being from the two nitrogen systems.

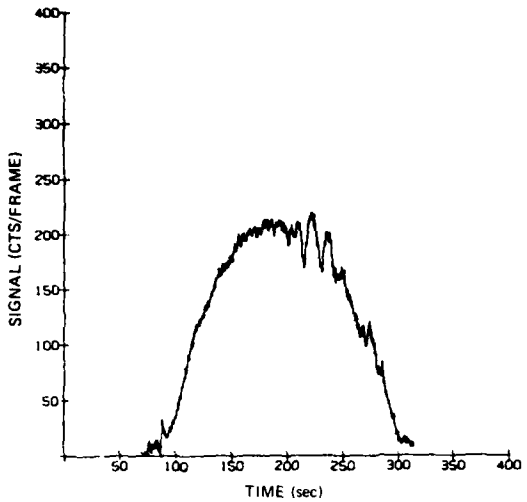

Figure 46. PA1 Signal Attributed to N_2 2P(2,0) vs Time

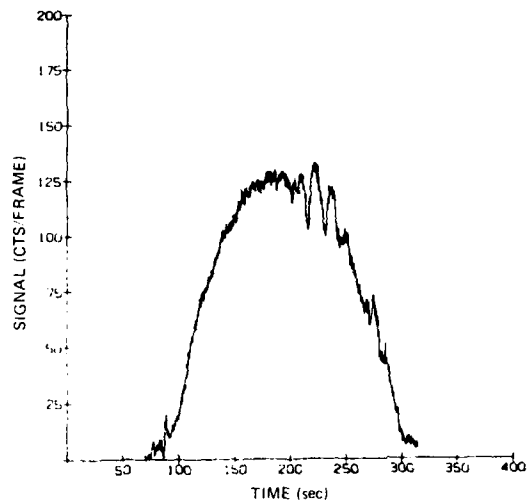

Figure 47. PA1 Signal Attributed to N_2 2P(3,1) vs Time

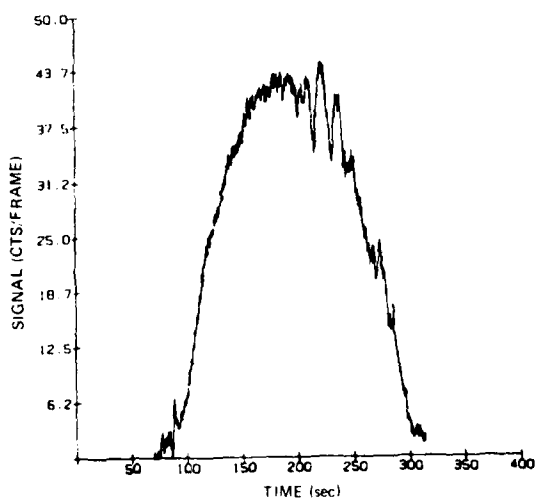

Figure 48. PA1 Signal Attributed to N_2 2P(4,3) vs Time

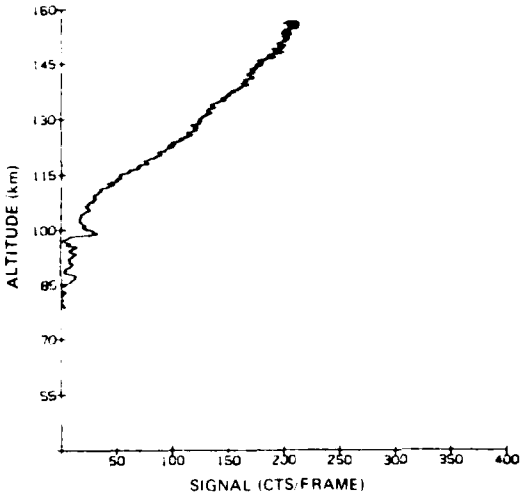

Figure 49. PA1 Signal Attributed to N_2 2P(2, 0) vs Altitude (Upleg)

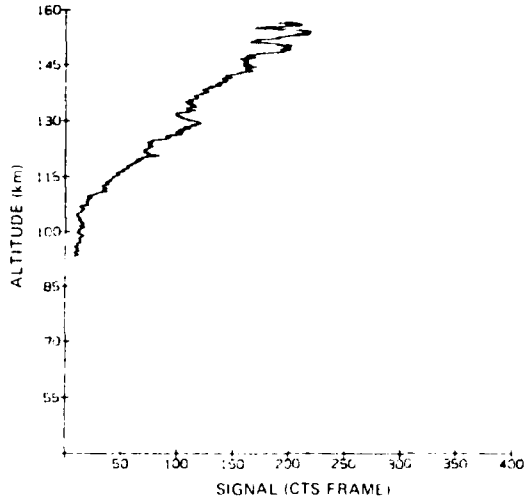

Figure 50. PA1 Signal Attributed to N_2 2P(2, 0) vs Altitude (Downleg)

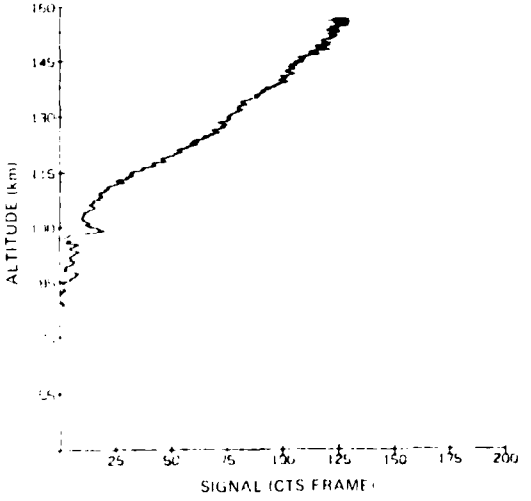

Figure 51. PA1 Signal Attributed to N_2 2P(3, 1) vs Altitude (Upleg)

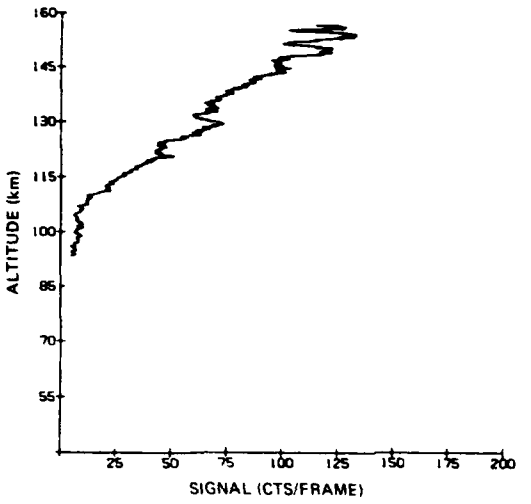

Figure 52. PA1 Signal Attributed to N_2 2P(3, 1) vs Altitude (Downleg)

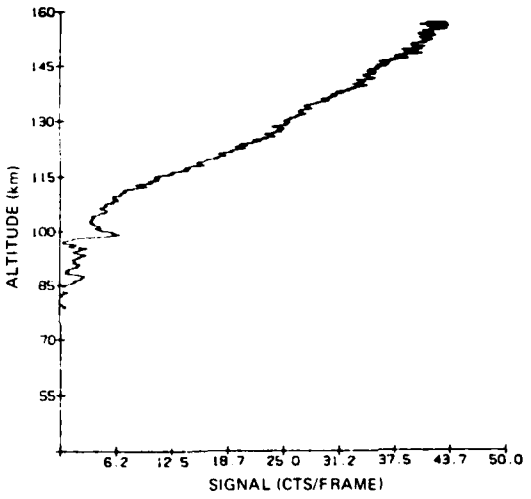

Figure 53. PA1 Signal Attributed to N_2 2P(4, 3) vs Altitude (Upleg)

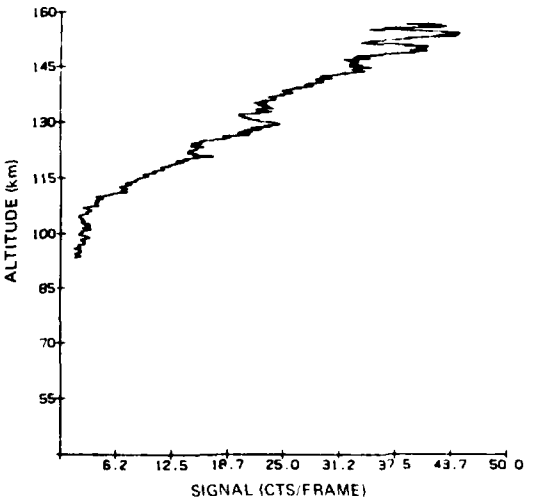

Figure 54. PA1 Signal Attributed to N_2 2P(4, 3) vs Altitude (Downleg)

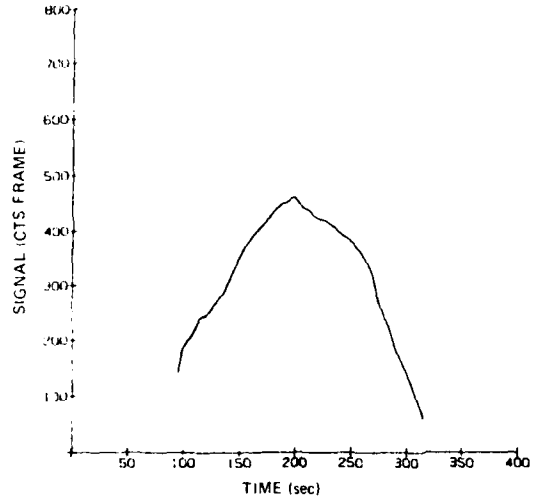

Figure 55. PA1 Signal Attributed to N_2 VK(0, 7) vs Time

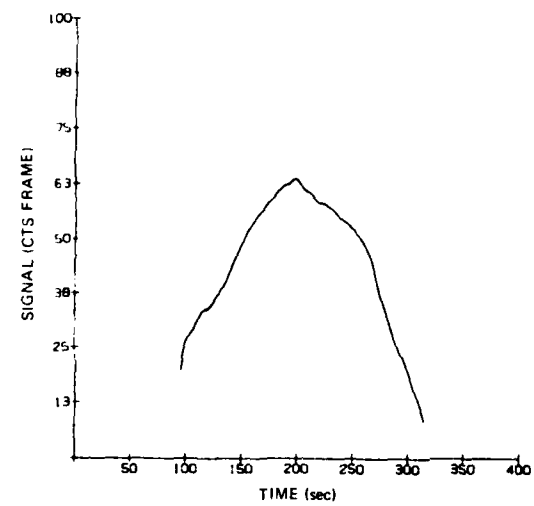

Figure 56. PA1 Signal Attributed to N_2 VK(1, 8) vs Time

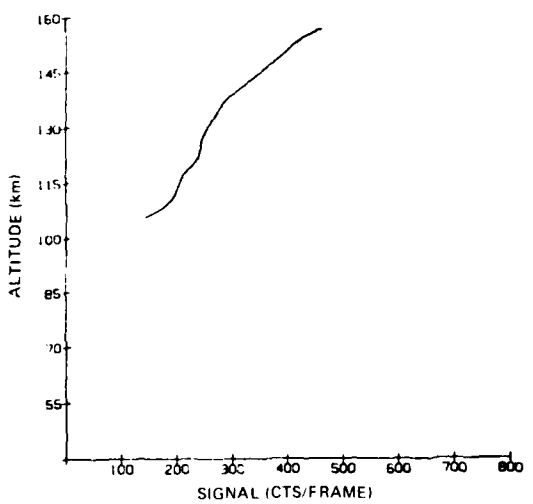

Figure 57. PA1 Signal Attributed to N_2 VK(0, 7) vs Altitude (Upleg)

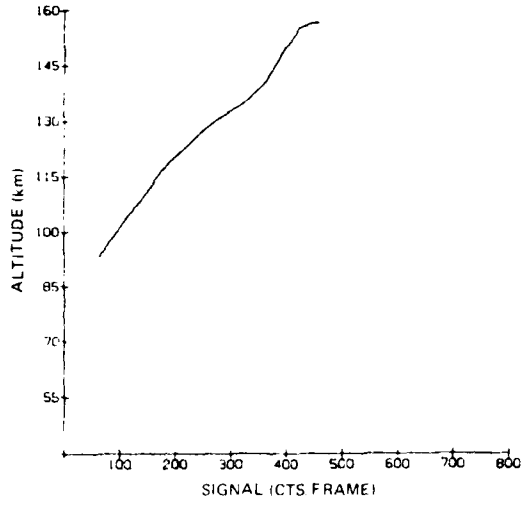

Figure 58. PA1 Signal Attributed to N_2 VK(0, 7) vs Altitude (Downleg)

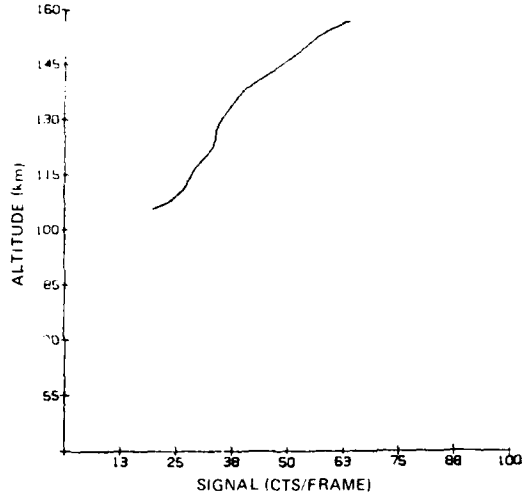

Figure 59. PA1 Signal Attributed to N_2 VK(1, 8) vs Altitude (Upleg)

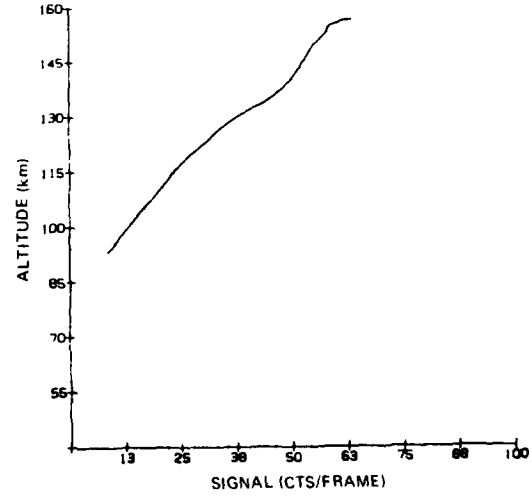

Figure 60. PA1 Signal Attributed to N_2 VK(1, 8) vs Altitude (Downleg)

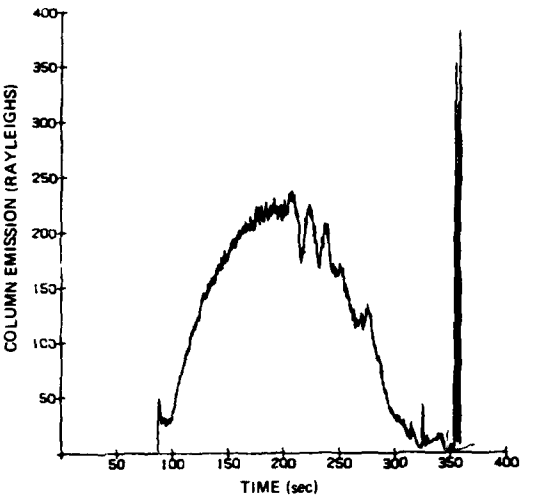

Figure 61. Apparent Column Emission of OI (2972) vs Time From Photometer PA1

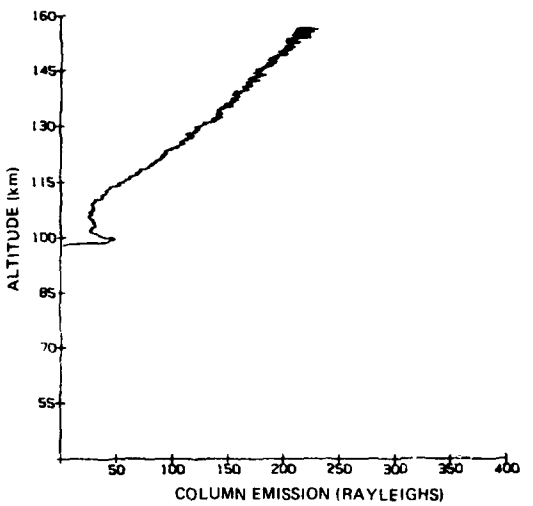

Figure 62. Apparent Column Emission of OI (2972) vs Altitude From Photometer PA1 (Upleg)

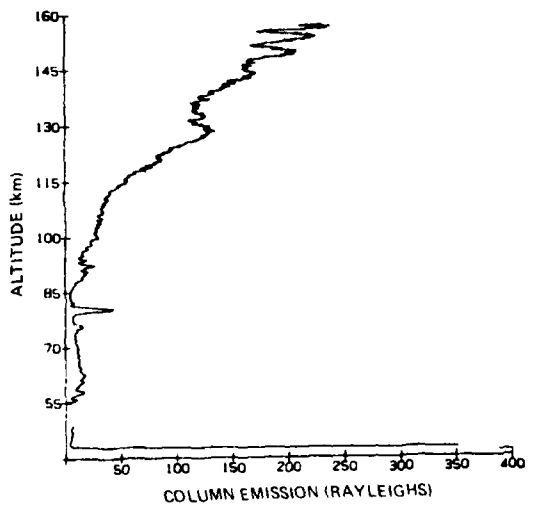

Figure 63. Apparent Column Emission of OI (2972) vs Altitude From Photometer PA1 (Downleg)

Table 5. Contribution to the PA1 Signal From OI N_2 2P and N_2 VK Emissions at Apogee

Feature	Signal (cts/frame)	Percent
OI $^1S - ^3P$	950	52
N_2 2P(2, 0)	210	11
N_2 2P(3, 1)	125	7
N_2 2P(4, 3)	42	2
N_2 VK(0, 7)	460	25
N_2 VK(1, 8)	63	3

5.5 H_β (4861 Å)

Observations of hydrogen line emissions are used to measure the amount of proton involvement in an aurora.[17] Although H_β is a weaker line than H_α, it particularly well suited for measurement with a rocket-borne filter photometer because it is reasonably well isolated from other auroral emissions, whereas H_α is blended with bands of the N_2 1st positive system. There is, however, an underlying continuum which must be measured separately and subtracted from the total signal in the H_β photometer to obtain the column emission rate due to H_β alone.

The line is strongly Doppler shifted toward shorter wavelengths and broadened as a result of the protons streaming into the atmosphere with considerable velocity along the earth's magnetic field lines. Zwick and Shepherd[18] recorded typical profiles looking both in the zenith and horizon directions. We used their typical zenith profiles as shown in Figure 64 to determine the relative band response of H_β with photometer PF4. The total signal observed by the upward-viewing photometer PF4 may be considered as the sum of the H_β emission and the underlying continuum, namely,

$$S(PF4, z) = C_o(PF4) \left[R(H_\beta, z) \int \beta_\lambda(\lambda)\, \eta(PF4, \lambda)\, d\lambda + R_\lambda(z)\, W_{eq}(PF4) \right], \quad (15)$$

where $\beta_\lambda(\lambda)$ is the Doppler-broadened spectral distribution of intensity over the line, $\eta(PF4, \lambda)$ is the relative spectral response of the photometer, and R_λ is the spectral radiance of the underlying continuum. R_λ was determined by means of the signal

17. Omholt, H. (1971) The Optical Aurora, Springer-Verlag, New York.

18. Zwick, H. H., and Shepherd, G. G. (1963) Some observations of hydrogen-line profiles in the aurora, J. Atmos. Terr. Phys. 25:604.

in a companion photometer, PF5, which observed only continuum radiation in a 45 Å interval around 5080 Å.

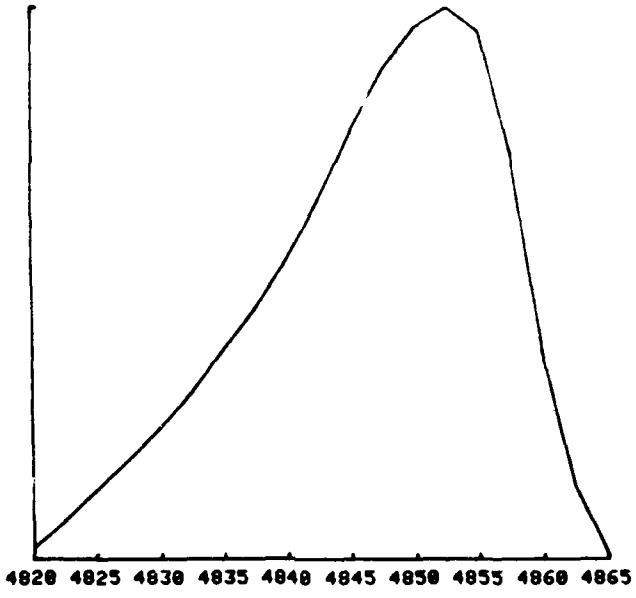

Figure 64. Typical Zenith Profiles of H_β
(See Reference 19)

The apparent column emission for H_β emission is shown vs time in Figure 65 and vs altitude for the upleg and downleg portions of the flight in Figures 66 and 67. The emission drops sharply from 80R below 100 km to only 15 R at apogee (156 km). It does not show the structure which appears in both the N_2^+ 1st negative and N_2 2nd positive altitude profiles.

19. Esther, R.H. (1968) Spectral intensity ratios in proton-induced auroras, J. Geophys. Res. 73:119.

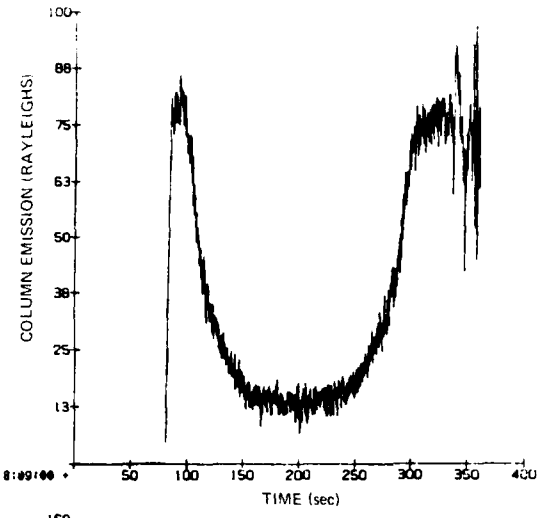

Figure 65. Apparent Column Emission of H_β vs Time From Photometer PF4

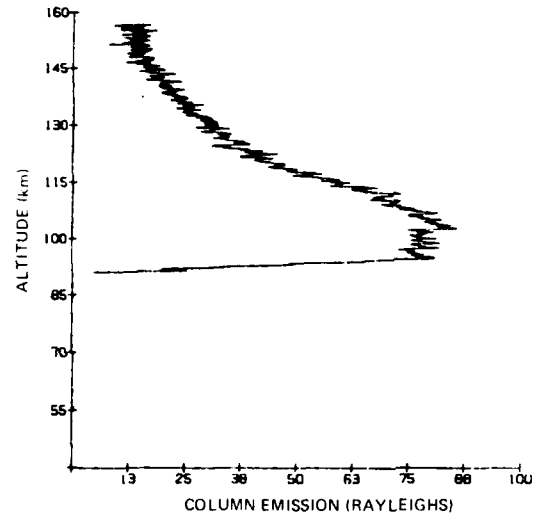

Figure 66. Apparent Column Emission of H_β vs Altitude From Photometer PF4 (Upleg)

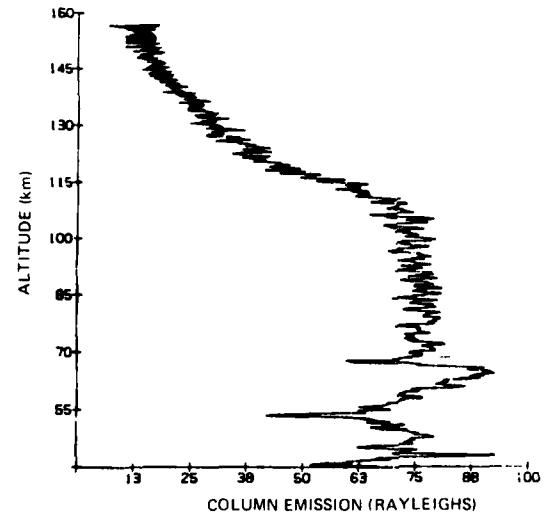

Figure 67. Apparent Column Emission of H_β vs Altitude From Photometer PF4 (Downleg)

The intensity ratio between H_β and the 1st negative bands of N_2^+ may be used to judge the relative contribution from primary protons and electrons in producing an aurora.[17] Eather[19] made measurements of the ratio $\lambda 3914/H_\beta$ of what were believed to be typical hydrogen arcs over Fort Churchill early in the evening (1730 - 2030 LT), and observed at zenith angles between 60° to 75° to the north, close to the magnetic horizon plane. This time was selected because there was rarely any trace of bright or structured aurora which would indicate electron precipitation. The range of $\lambda 3914/H_\beta$ was between 10 and 17.5 with an average value of 14 ± 2. This is in reasonable agreement with theoretical calculations by Omholt,[17] who concludes that when the $\lambda 3914/H_\beta$ ratio approaches 10 to 14, it is likely that the aurora is produced predominantly by protons. The ratio of $\lambda 3914/H_\beta$ observed here ranged between 16, looking upward from 85 km, to about 20 at apogee. This indicates that this aurora was produced to a substantial degree by protons.

5.6 Continuum (5080 Å)

Measurement of the night-sky continuum is of interest not only because it underlies H_β and is necessary to accurately assess the proportion of H_β in the signal from photometer PF4, but also because it is generally attributed to the air afterglow continuum which results from the reaction of nitric oxide and atomic oxygen to form nitrogen dioxide.[20, 21, 22] The NO + O reaction is a laboratory standard of chemiluminescence and has been subject to numerous investigations related to the complicated reaction mechanism as well as to the absolute photon production rate.[23, 24] An excellent review of these studies as they relate to inferring NO concentrations in an aurora from optical measurements of the afterglow continuum is given by Witt et al.[21]

The apparent column emission of the night-sky continuum at 5080 Å is shown vs time for the upward-viewing photometer PF5 in Figure 68 and for the downward-viewing photometer PA6 in Figure 69. The same data is plotted as a function of altitude for the upleg and downleg portions of the flight in Figures 70-73. The sharp peaks which are seen when viewing downward prior to 100 sec (Figure 69) and at altitudes less than 110 km on upleg (Figure 72) are due to the photometers viewing the lights from the Fairbanks Airport as the rocket was tipped over to eject the nose cone, and to the fortuitous observations of the launch of the second rocket in the series of four which were launched as part of the auroral-E program.

(Due to the large number of references cited above, they will not be listed here. See References, page 59.)

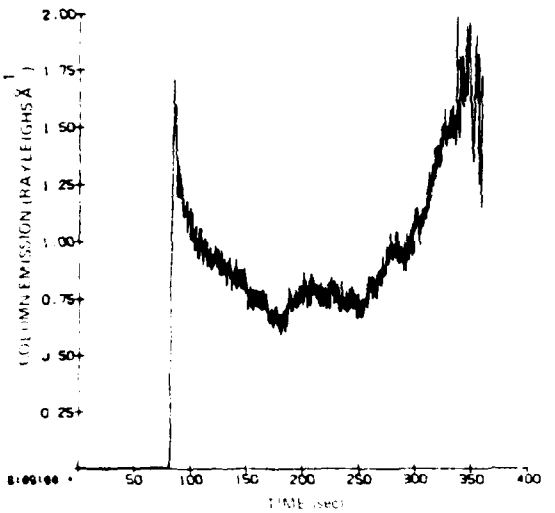

Figure 68. Apparent Column Emission of the Night-Sky Continuum vs Time From Photometer PF5

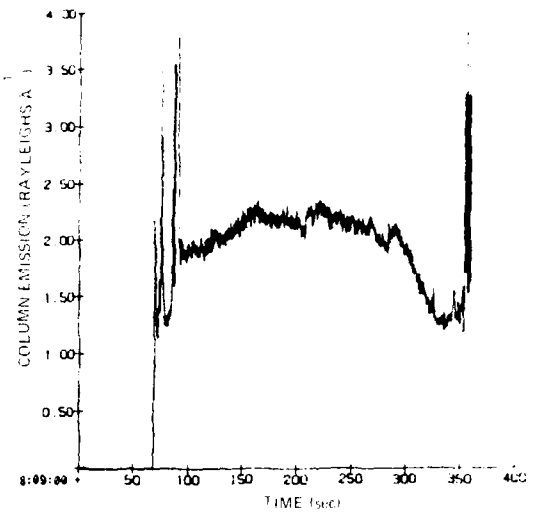

Figure [illegible] Apparent Column Emission of the Night-Sky Continuum vs Time From Photometer PA6

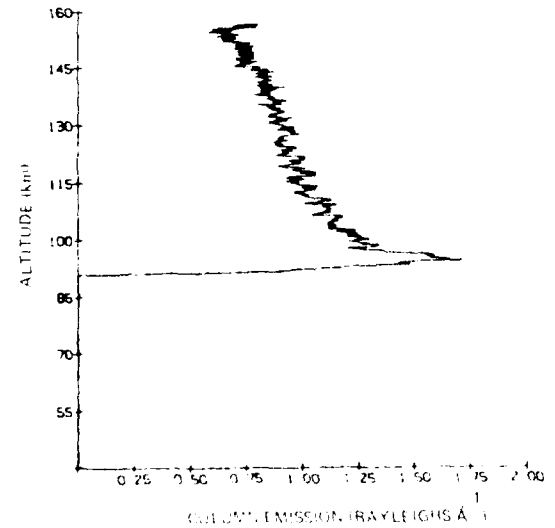

Figure 70. Apparent Column Emission of the Night-Sky Continuum vs Altitude From Photometer PF5 (Upleg)

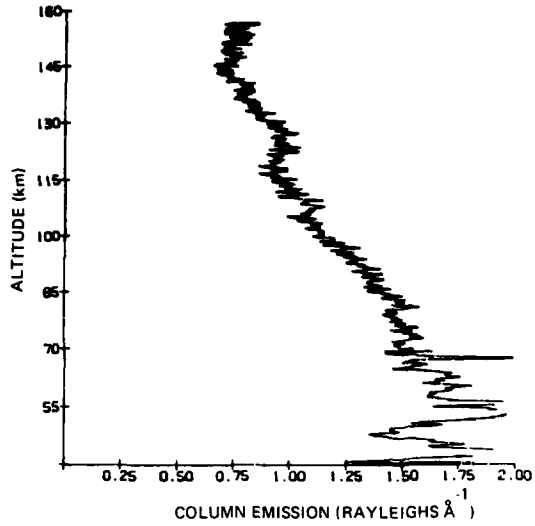

Figure 71. Apparent Column Emission of the Night-Sky Continuum vs Altitude From Photometer PF5 (Downleg)

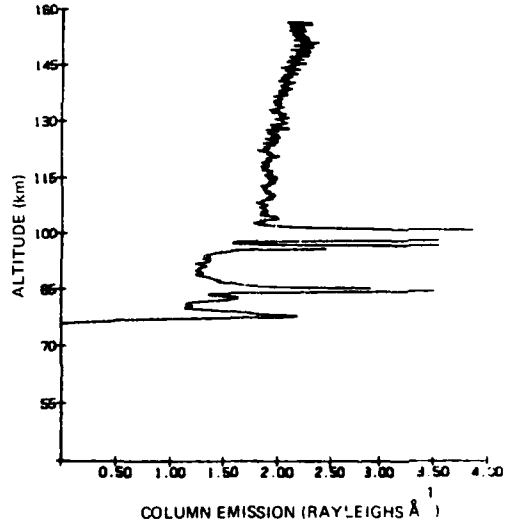

Figure 72. Apparent Column Emission of the Night-Sky Continuum vs Altitude From Photometer PA6 (Upleg)

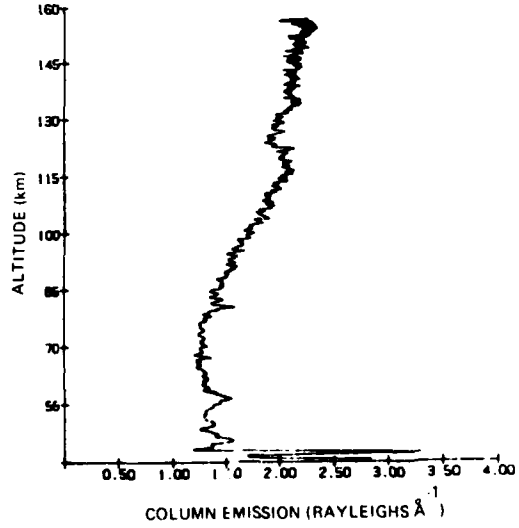

Figure 73. Apparent Column Emission of the Night-Sky Continuum vs Altitude From Photometer PA6 (Downleg)

The downward-viewing photometer measured a radiance of about 1.3 $R\text{Å}^{-1}$ below 80 km. We interpret this signal as due to ground return. Both the upward-viewing and downward-viewing photometers measure 0.6 ± 0.1 $R\text{Å}^{-1}$ from the auroral layer between 85 and 130 km, in reasonable agreement with measurements of Sharp[22] who reported intensities of the order of 1.0 $R\text{Å}^{-1}$ at 5200 Å.

The sum of the apparent column emission of the upward-viewing and downward-viewing photometers is shown vs time in Figure 74 and vs altitude on upleg and downleg in Figures 75 and 76. The sum shows emission rates between 2.8 and 3.0 $R\text{Å}^{-1}$, which includes the ground return of 1.3 $R\text{Å}^{-1}$. The sky above the emitting layer contributes about 0.8 $R\text{Å}^{-1}$.

6. COMPARISON OF N_2^+ 1N AND N_2 VK TO N_2 2P

Plots of the ratio of the N_2^+ to N_2 2P emissions are useful because, although both systems are excited by electron impact of neutral, ground-state molecular nitrogen, there is a striking difference in the excitation cross-sections of the two systems. Excitation of the N_2^+ 1N system is peaked at 100 eV and falls off only very slowly with increasing energy, whereas the cross-section for excitation of the N_2 2P system is sharply peaked at 15 eV. Comparison of the two bands, then, is a measure of the difference in the electron spectrum with altitude and is independent of both the nitrogen profile and variations in intensity. The profile of N_2^+ 1N(0, 0)/N_2 2P(0, 0) vs altitude is shown in Figures 77 and 78 for the upleg and downleg portions of the flight. The ratio declines from about 2.5 when viewing upward below 115 km to 2.1 when viewing from apogee (156 km). This contrasts with the observations of Feldman and Doering[25] who found that the ratio was nearly independent of altitude in a 40 kR (λ5577) aurora. The difference may be related to the degree of proton excitation in the production of the auroral-E layer.

Figures 79 and 80 show the ratio of N_2 VK(0, 6) to N_2 2P(0, 0) emission. Although the $A\ ^3\Sigma_u^+$ is produced predominantly by cascading from upper levels, primarily from the C state through emission of the 2P system, the process is complicated by transitions between large numbers of vibrational levels. The ratio declines from a maximum of 0.5 at apogee to a minimum of 0.25 at 105 km, increasing to 0.32 below 85 km. The VK system is highly quenched below 145 km because of the long lifetime (≈ 2 s) of the $A\ ^3\Sigma_u^+$ state. This explains the steady rise in the ratio of the column emission of VK/2P as a function of altitude. Explanation of the minimum at 105 km will require more detailed calculations.

25. Feldman, P. D., and Doering, J. P. (1975) Auroral electrons and the optical emissions of nitrogen, J. Geophys. Res. 80:2808.

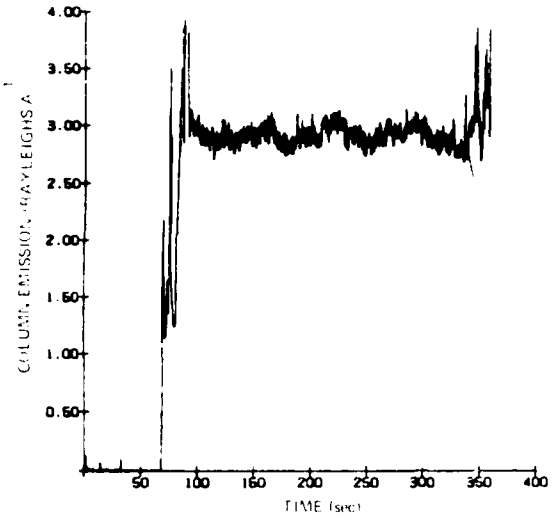

Figure 74. Sum of Apparent Column Emission of the Night-Sky Continuum vs Time From Photometers PF5 and PA6

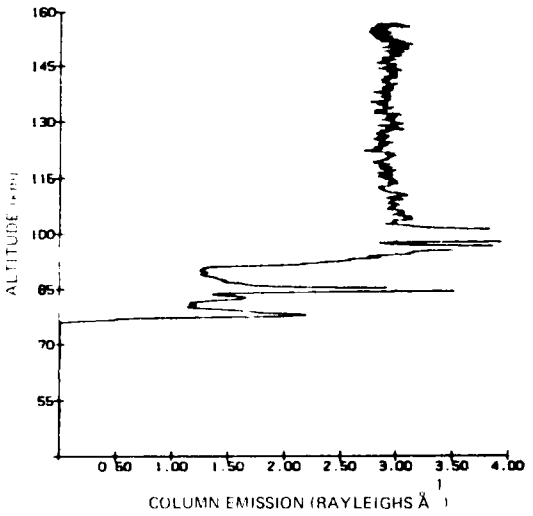

Figure 75. Sum of Apparent Column Emission of the Night-Sky Continuum vs Altitude From Photometers PF5 and PA6 (Upleg)

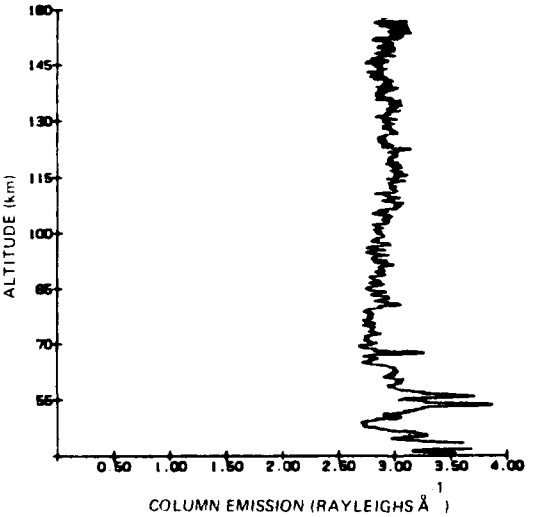

Figure 76. Sum of Apparent Column Emission of the Night-Sky Continuum vs Altitude From Photometers PF5 and PA6 (Downleg)

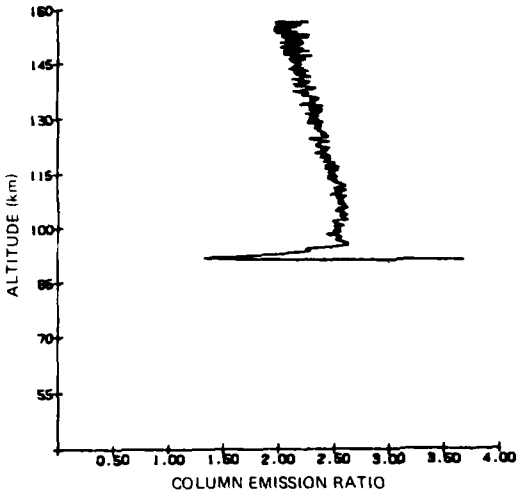

Figure 77. Ratio of Column Emission of N_2^+ 1N(0, 0) to N_2 2P(0, 0) vs Altitude as Measured by Photometers PF3 and PF2 (Upleg)

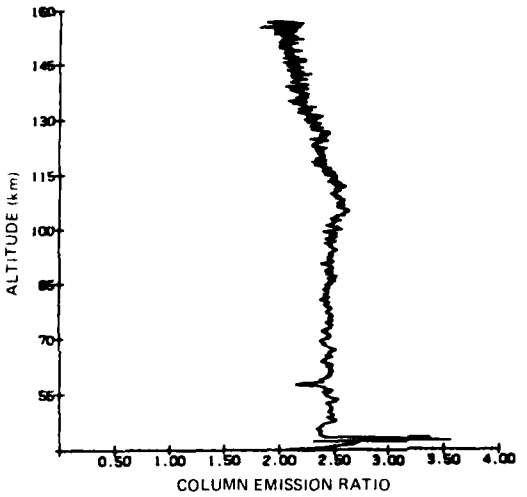

Figure 78. Ratio of Column Emission of N_2^+ 1N(0, 0) to N_2 2P(0, 0) vs Altitude as Measured by Photometers PF3 and PF2 (Downleg)

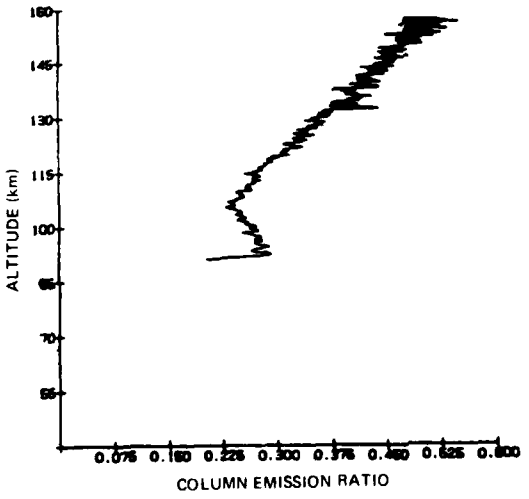

Figure 79. Ratio of Column Emission of N_2 VK(0, 6) to N_2 2P(0, 0) vs Altitude as Measured by Photometers PF1 and PF2 (Upleg)

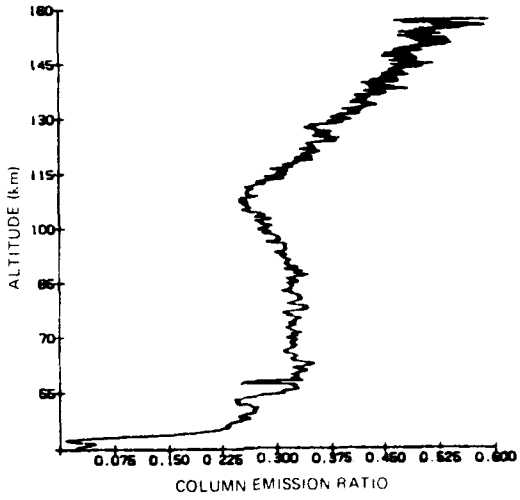

Figure 80. Ratio of Column Emission of N_2 VK(0, 6) to N_2 2P(0, 0) vs Altitude as Measured by Photometers PF1 and PF2 (Downleg)

References

1. Dick, K.A., and Fastie, W.G. (1969) Up-down photometers for auroral profile studies, Applied Optics 8:2457.

2. Chamberlain, J.W. (1961) Physics of the Aurora and Airglow, Academic Press, New York, p. 569.

3. Torr, M.R., Espy, P.E., and Wraight, P. (1981) Intercalibration of Instrumentation Used in the Observation of Atmospheric Emissions: Second Progress Report 1981, Report No. CASS-101, Center for Atmospheric and Space Sciences, Utah State University, UMC 41, Logan, Utah 84322.

4. Huffman, R.E., LeBlanc, F.J., Larrabee, J.C., and Paulsen, D.E. (1980) Satellite vacuum ultraviolet and auroral observations, J. Geophys. Res. 85:2201.

5. Bates, D.R. (1949) The intensity distribution in the nitrogen band systems emitted from the earth's upper atmosphere, Proc. Roy. Soc. (London), Ser. A. 196:217.

6. Shemansky, D.E., and Broadfoot, A.L. (1971) Excitation of N_2 and N_2^+ systems by electrons. I: Absolute transition probabilities, J. Quant. Spectrosc. Radiat. Transfer 11:1385.

7. Borst, W.L., and Zipf, E.C. (1970) Cross-section for the 0,0 1N N_2^+ band from threshold to 3 keV, Phys. Rev. A1:834.

8. Huber, K.P., and Herzberg, G. (1979) Molecular Spectra and Molecular Structure IV. Constants of Diatomic Molecules, Van Nostrand Reinhold Company, New York.

9. Kovacs, I. (1969) Rotational Structure in the Spectra of Diatomic Molecules, American Elsevier Publishing Co., Inc., New York.

10. Herzberg, G. (1950) Molecular Spectra and Molecular Structure I. Spectra of Diatomic Molecules, D. Van Nostrand Company, Princeton, New Jersey.

11. Shemansky, D.E., and Broadfoot, A.L. (1971) Excitation of N_2 and N_2^+ systems by electrons. II: Excitation cross-sections and N_2 IPG low pressure afterglow, J. Quant. Spectrosc. Radiat. Transfer 11:1401.

12. [illegible]

13. [illegible]

14. [illegible]

15. [illegible]

16. [illegible]

17. Omholt, A. (1971) The Optical Aurora, Springer-Verlag, New York.

18. Zipf, E.C., and Shepherd, G.G. (1963) Some observations of oxygen emission profiles in the aurora, J. Atmos. Terr. Phys. 25:504.

19. Luther, R.H. (1968) Spectral intensity ratios in proton-induced auroras, J. Geophys. Res. 73:119.

20. Donahue, T.M. (1974) An upper limit to the product of NO and O densities from 105 to 120 km, J. Geophys. Res. 83:4373.

21. Witt, G., Rose, J., and Llewellyn, E.J. (1961) The airglow continuum at high latitudes—an estimate of the NO concentration, J. Geophys. Res. 66:24.

22. Sharp, W.E. (1978) NO_2 continuum in aurora, J. Geophys. Res. 83:4373.

23. Becker, K.H., Groth, W., and Thran, D. (1972) The mechanism of the air afterglow NO + O → NO_2 + $h\nu$, Chem. Phys. Lett. 15:215.

24. Kaufman, F. (1972) The air afterglow revisited, in Chemiluminescence and Bioluminescence, edited by M.J. Cormier, D.M. Hercules, and J. Lee, Plenum, New York, p. 83.

25. Feldman, P.D., and Doering, J.P. (1975) Auroral electrons and the optical emissions of nitrogen, J. Geophys. Res. 80:2808.

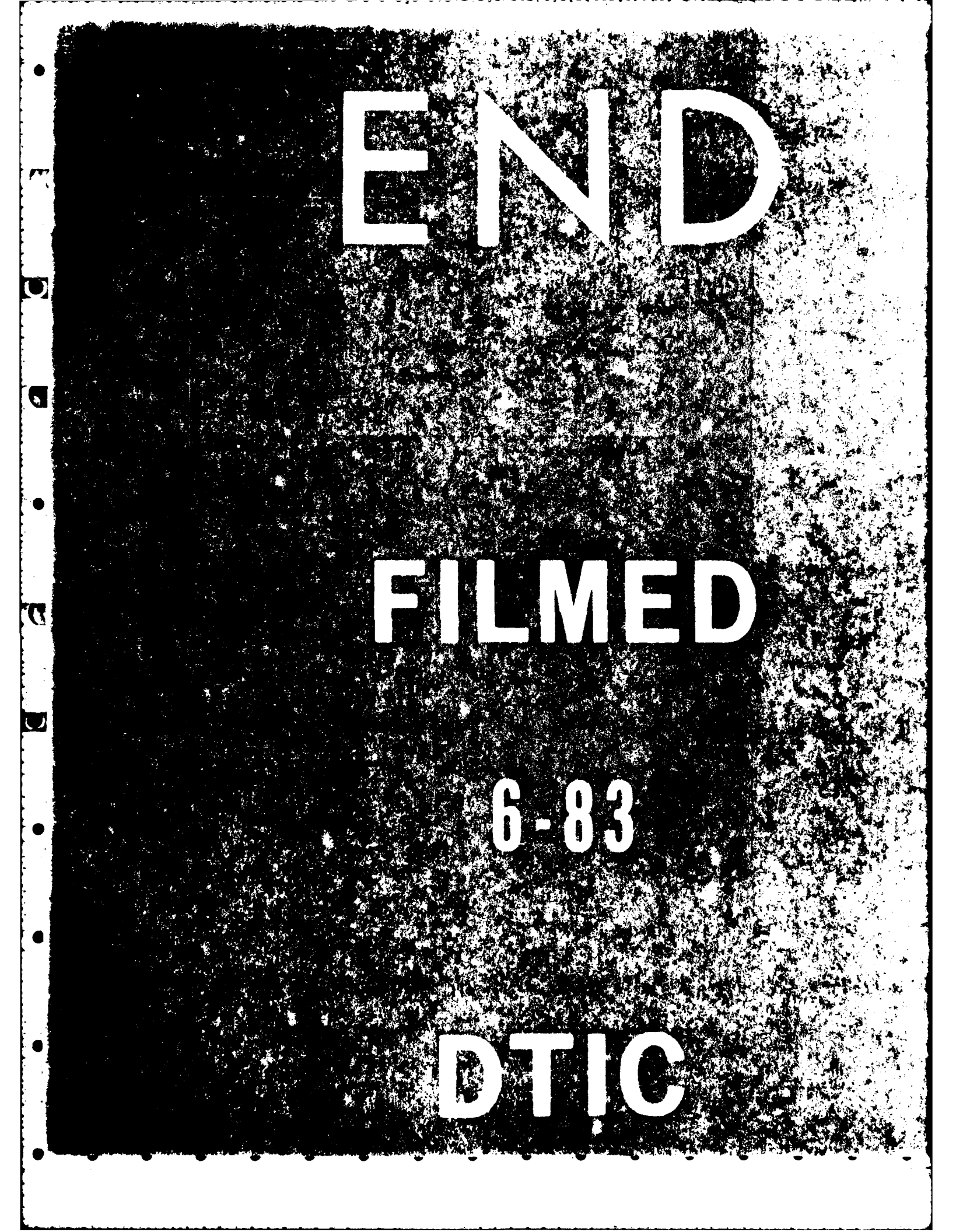
END
FILMED
6-83
DTIC